d·Collection

Non-invasive Continuous Arterial Blood Pressure Monitoring System: Large Population Models and Single Chest-worn Device

대규모 인구 모델과 단일 가슴 착용형 장치를 활용한 비침습적 연속 동맥 혈압 모니터링 시스템

2021 년 2 월

서울대학교 대학원

협동과정 바이오엔지니어링 전공

양 승 만

Ph. D. Dissertation

Non-invasive Continuous Arterial Blood Pressure Monitoring System: Large Population Models and Single Chest-worn Device

지도교수 김 희 찬

이 논문을 공학박사 학위논문으로 제출함
2020 년 12 월

서울대학교 대학원
협동과정 바이오엔지니어링 전공
양 승 만

양승만의 공학박사 학위논문을 인준함
2020 년 12 월

위 원 장	김 희 수	(인)
부위원장	김 희 찬	(인)
위 원	이 해 영	(인)
위 원	이 사 람	(인)
위 원	노 승 우	(인)

i

Non-invasive Continuous Arterial Blood Pressure Monitoring System: Large Population Models and Single Chest-worn Device

BY

SEUNGMAN YANG

FEBRUARY 2021

INTERDISCIPLINARY PROGRAM IN

BIOENGINEERING

THE GRADUATE SCHOOL

SEOUL NATIONAL UNIVERSITY

Non-invasive Continuous Arterial Blood
Pressure Monitoring System: Large
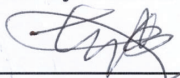Population Models and Single Chest-worn
Device

BY

SEUNGMAN YANG

INTERDISCIPLINARY PROGRAM IN
BIOENGINEERING
THE GRADUATE SCHOOL
SEOUL NATIONAL UNIVERSITY

THIS DISSERTATION IS APPROVED FOR THE
DEGREE OF DOCTOR OF PHILOSOPHY

DECEMBER 2020

Approved by Thesis Committee:

Professor _____ Chairman
Hee Soo Kim

Professor _____ Vice chairman
Hee Chan Kim

Professor _____ Member
Hae Young Lee

Professor _____ Member
Saram Lee

Ph.D _____ Member
Seungwoo Noh

ii

ABSTRACT

Non-invasive Continuous Arterial Blood Pressure Monitoring System: Large Population Models and Single Chest-worn Device
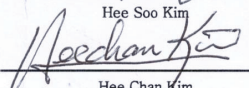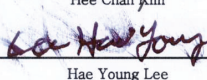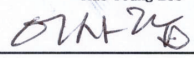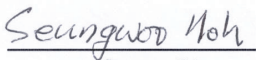
Seungman Yang

Interdisciplinary Program in Bioengineering

The Graduate School

Seoul National University

As non-invasive continuous blood pressure monitoring (NCBPM) has gained wide attraction in the recent decades, many studies on blood pressure (BP) estimation using pulse transit time (PTT), pulse arrival time (PAT), and characteristics extracted from the morphology of photoplethysmogram (PPG) waveform as indicators of BP have been conducted. However, most of the studies have used small homogeneous subject pools to generate models of BP, which led to inconsistent results in terms of accuracy. Furthermore, the previously proposed modalities to measure BP indicators are questionable in terms of practicality, and lack the potential for being utilized in daily life.

The first goal of this thesis is to develop a BP estimation model with clinically valid accuracy using a large pool of heterogeneous subjects undergoing various surgeries. This study presents analyses of BP estimation methods using 2.4 million cardiac cycles of two commonly used non-invasive biosignals, electrocardiogram (ECG) and PPG, from 1376 surgical patients. Feature selection methods were used to determine the best subset of predictors from a total of 42 including PAT, heart rate, and various PPG morphology

features. BP estimation models were constructed using linear regression, random forest, artificial neural network (ANN), and recurrent neural network (RNN), and the performances were evaluated. 28 features out of 42 were determined as suitable for BP estimation, in particular two PPG morphology features outperformed PAT, which has been conventionally seen as the best non-invasive indicator of BP. By modelling the low frequency component of BP using ANN and the high frequency component using RNN with the selected predictors, mean errors of 0.05 ± 6.92 mmHg for systolic blood pressure (SBP), and -0.05 ± 3.99 mmHg for diastolic blood pressure (DBP) were achieved. External validation of the model using another biosignal database consisting of 334 intensive care unit patients led to similar results, satisfying three international standards concerning the accuracy of BP monitors. The results indicate that the proposed method can be applied to large number of subjects and various subject phenotypes.

The second goal of this thesis is to develop a wearable BP monitoring system, which facilitates NCBPM in daily life. Most previous studies used two or more modules with bulky electrodes to measure biosignals such as ECG and PPG for extracting BP indicators. In this study, a single wireless chest-worn device measuring ECG and PPG simultaneously was developed. Biosignal data from 25 healthy subjects measured by the developed device were acquired, and the BP estimation model developed above was tested on this data after applying a transfer function mapping the chest PPG morphology features to the corresponding finger PPG morphology features. The model yielded mean errors of 0.54 ± 7.47 mmHg for SBP, and 0.29 ± 4.33 mmHg for DBP, again satisfying the three standards for the accuracy of BP monitors. The results indicate that the proposed system can be a stepping stone to the realization of mobile NCBPM in daily life.

In conclusion, the clinical validity of the proposed system was checked in three different datasets, and it is a practical solution to NCBPM due to its non-occlusive form as a single wearable device.

CONTENTS

List of Tables

List of Figures

CHAPTER 1

General Introduction

1.1 Need for Non-invasive Continuous Blood Pressure Monitoring (NCBPM)

According to the World Health Organization (WHO), cardiovascular diseases (CVD) are the leading causes of worldwide mortality, representing a heavy socioeconomic burden for the affected individuals [1]. Hypertension, or abnormally high blood pressure (BP), is a major predictor of CVD and is often a therapeutic target for CVD patients [2-7]. Hypertension is defined as systolic blood pressure (SBP) of 130 mmHg or higher, diastolic blood pressure (DBP) of 80 mmHg or higher, or currently taking medication to lower high BP [8]. According to the National Center for Health Statistics (NCHS), the prevalence of hypertension was 45.4 % among adults in survey period 2017-2018 [9]. Although hypertension can be prevented through proper monitoring and management of BP [10], there has been a lack of adequate devices for early diagnosis and prevention of hypertension.

BP can be mostly accurately measured through the insertion of a catheter into an artery (usually radial, femoral, or brachial), and it is regarded as the gold standard measurement method in clinics. However, since this method is invasive, it can be only employed in human under intensive care medicine, anesthesiology, or for research purposes. As a non-invasive method, the auscultatory method is the predominant method of clinical measurement, which

detects Korotkoff sounds to measure BP using sphygmomanometer composed of an inflatable cuff placed around the upper arm [11]. Similar to auscultatory method, the oscillometric method uses a sphygmomanometer to measure BP. It observes cuff pressure oscillations, and automatically interpret them to measure BP. As it requires less skill than the auscultatory method, this technique has become the most popular method, widely used in homes and clinics. However, these cuff-based non-invasive methods inflate the cuff pressure above SBP to occlude the artery of the upper arm, which may cause temporary pain or ischemia during the measurements. Moreover, they can provide only a single discrete BP measurement.

Recent studies have shown that a single discrete BP measurement, generally performed in clinical settings with a conventional cuff-type oscillometric device, can be misleading [10, 12, 13], and that methods which can observe circadian fluctuations of BP, such as ambulatory BP monitoring (ABPM), are required for accurate diagnosis of hypertension [13-15]. However, the periodic oscillometric operation of ABPM devices lead to lowered quality of life for the users [16, 17], and due to this inconvenience, it is not optimal for non-invasive continuous BP monitoring (NCBPM). As the importance of ambulatory blood pressure has been stressed in many recent studies on the topic [13, 15], it can be deduced that while continuous monitoring is required in daily life for accurate diagnosis of BP and cardiovascular health, the conventional

cuff-based method is not practical due to its inconvenient and cumbersome

nature.

1.2 Previous Studies for NCBPM

In light of the need for NCBPM, multiple indirect approaches to BP estimation have been developed throughout the last few decades, and pulse wave velocity (PWV) based methods have gained the most interest [18-27]. Starting with Geddes et al. in 1981 [20], a wide range of studies using PWV and related parameters have been published. PWV is defined as the velocity at which an arterial pulse travels in an artery from a proximal point to a distal point. Through the well-known arterial compliance modelling of BP [28, 29], PWV is affected by physiological variations of the arterial vessels, which is closely related to BP. According to Moens-Korteweg equation which models the relationship between arterial elastance and PWV assuming an artery as an elastic tube, PWV can be represented as followed [30-32]:

$$PWV = \sqrt{\frac{Eh}{2\rho r}} \tag{1}$$

where E is arterial elastance, h is vessel wall thickness, r is vessel radius, and ρ is blood density. The equation states that PWV is proportional to the square root of the arterial elastance. Meanwhile, the arterial elastance is exponentially correlated with BP by Hughes equation which empirically relates BP to the arterial elastance as followed [33]:

$$E = E_0 e^{\alpha \cdot BP} \tag{2}$$

where E_0 and α are subject-specific parameters. The combination of the two equations thus gives the relationship between BP and PWV as followed:

$$BP = \frac{2}{\alpha} lnPWV + \frac{1}{\alpha} ln\frac{2\rho r L^2}{E_0 h} \tag{3}$$

Consequently, PWV is physiologically linked to BP through the arterial elastance. PWV can be approximated using its surrogates pulse transit time (PTT), which is the time delay for the arterial pulse to propagate between two arterial sites. Although numerous studies have tried to establish a BP estimation method using PTT, most studies have used pulse arrival time (PAT) instead, due to the ease of measurement [19, 34-38]. PAT is defined as the time delay from the R-peak of the electrocardiogram (ECG) to a point on distal pulse waveform such as the photoplethysmogram (PPG) [39]. Although some studies have shown remarkable results in NCBPM using PAT and/or PTT methods [19, 21, 27, 40-42], in terms of accuracy, there are still widely varying results [37, 43, 44].

In order to find some new predictors associated with BP to improve the estimation accuracy, many researchers have attempted to analyze the morphology of the PPG waveform [45-51]. PPG is an optical technique that measures the changes of blood volume in the central or peripheral blood vessels. PPG is measured by illuminating a light source to the tissue, and detecting

transmitted or reflected light by a photodetector. Since the PPG waveform should reflect both the ejection of blood from the heart and the conditions of the peripheral artery [52], the characteristics from the morphology of PPG waveforms may contain physiologically meaningful information about BP. Therefore, many previous studies have been conducted with an attempt to find various indicators extracted from the magnitude and temporal variation information contained in the PPG waveform, or the derivatives of the PPG waveform in both time domain and frequency domain for BP estimation [45-51]. Some commonly used PPG morphology features include (1) magnitude variation information in the PPG waveform: the intensity of the specific characteristic points such as valley point and peak point of PPG, and PPG intensity ratio of PPG peak intensity to PPG valley intensity [53]; (2) temporal variation information in the PPG waveform: time delay from the valley point to the peak point of PPG (crest time) [54], and the pulse width at half of the pulse height (branch width) [55]; (3) area information in the PPG waveform: PPG characteristic value (PPGK) [56]; (4) slope information in the PPG waveform: the rate of wave front sloping (ascending slope) [57]; (5) information in the second derivative of PPG waveform (acceleration plethysmogram) [58]; (6) dimensionality reduction of the raw PPG waveform [59]. However, different characteristics were extracted from the PPG morphology for each study, and comprehensive understanding of the general

relationship between diverse PPG morphology features and BP was unavailable

yet.

1.3 Issues with Previous Studies

NCBPM has gained wide attraction in the recent decade and a growing number of methods are being developed for non-invasive BP estimation, but a probing into the published research reveals a key issue that researchers face in this area. As reported by Mukkamala et al. in a well-recognized review [39], most researchers tend to recruit a small number (n<100) of homogeneous subjects (usually young healthy males) for the development of BP estimation algorithm based on features extracted from non-invasive biosignals. However, these BP estimation models are not extendable for general use, and a comprehensive understanding of the general relationship between these predictors and BP was unavailable. These limitations extend to recent articles [60-65] beyond the ones covered in the review, and the validity of the methods developed with such limitations must be carefully assessed.

In several international standards for BP monitors, performance in terms of errors is not the only set of criteria for validating BP monitors, and there is a strict guideline on subject selection. For example, validation study subjects must include both normotensive and hypertensive subjects with varying ranges of baseline BP, and the number of subjects must be large enough for reliable validation. Due to these guidelines, researchers have turned to large biosignal databases for the development and analysis of BP estimation models [59, 68-71], with the most focus on Physionet Medical Information Mart for Intensive

Care (MIMIC) database due to its large size and accessibility [72, 73]. Kachuee *et al.* used approximately 1000 unique subjects from the MIMIC dataset and achieved acceptable results for DBP [59], and Wang *et al.* achieved more impressive results from the same database, but only used 72 subjects in total [71]. However, these databases are often collected from multiple sources, which restricts analyzing the dataset as a whole, since the variability in biosignal measurement modalities may cause time-domain inconsistencies in parameter extraction. In a recent study, Liang et al. demonstrated that inter-waveform analyses using MIMIC was leading to erroneous conclusions [74]. Therefore, to this day, it is unclear whether BP estimation methods can be applied to large subject pool with varying subject characteristics. In order to overcome the limitations mentioned above, the database used for BP estimation must be accessible and be consistently reliable in terms of inter-waveform alignment.

Another issue that researcher face in this area is that the measurement modalities for BP estimation proposed so far are not wearable and lack portability. In a practical perspective, in order to facilitate ubiquitous BP monitoring, the device should be wearable, such that the user will experience minimal discomfort. However, most previous studies have mainly focused on validating the use of BP indicators to estimate BP, enrooting bulky multi-module system designs due to the necessity of multi-site measurements for feature extraction. For example, in order to extract PAT as a BP indicator, most

studies have used two or more modules to detect both proximal and distal time references such as measuring ECG by attaching bulky electrodes to the chest and measuring PPG from the finger. This resulted the lack of a practical, light-weight wearable solution to daily monitoring of BP. Without a practical implementation that warrants light-weight design, it is unlikely that BP estimation will succeed in ubiquitous BP monitoring.

1.4 Thesis Objectives

In general, numerous studies of BP estimation using PAT or PTT, and various PPG morphology features as BP indicators have been conducted throughout the last few decades, and most of them reveal fundamental issues: 1) they have used small homogeneous subject pools to generate models of BP, which led to inconsistent results in terms of accuracy; 2) the modalities of most previous studies to measure biosignals for extracting BP indicators require two or more module system designs due to the necessity of multi-site measurements, which hinders their use in daily life monitoring. Therefore, the objective of this study is to develop the clinically usable BP estimation model analyzing large open biosignal databases, and to develop the wearable BP monitoring system using a single chest-worn device measuring ECG and PPG.

The first objective of this thesis is to assess the efficacy of PAT and various PPG morphology features as BP predictors from a large heterogeneous database, and to construct the clinically usable BP estimation models using the selected features. For this objective, we analyzed 2.4 million pairs of BP and 42 predictors including PAT, heart rate (HR), and various PPG morphology features extracted from a diverse group of 1376 surgical patients to evaluate the validity of the BP predictors using several feature selection methods. Then, BP estimation models based on the selected features constructed using linear

regression, random forest, artificial neural network, and recurrent neural network were evaluated (Chapter 2).

The second objective of this thesis is to develop the single wearable BP monitoring system, and to test the developed BP estimation model against the wearable device dataset. For this objective, we developed a wearable and unobtrusive single device that measured ECG and PPG simultaneously from the chest to enable ubiquitous and continuous monitoring of BP. This single unit hardware can provide users with utmost convenience in continuous BP monitoring. Since the characteristics of PPG waveform from the chest are different with those from the finger, we developed the transfer function mapping the chest PPG morphology features to the corresponding finger PPG morphology features. The chest PPG morphology features extracted from the wearable device dataset were translated to the finger PPG morphology features prior to inputting them to the BP estimation model. Then, the BP estimation model was tested against the wearable device dataset (Chapter 3).

CHAPTER 2

Non-invasive Continuous Arterial Blood Pressure Estimation Model in Large Population

2.1 Introduction

2.1.1 Electrocardiogram (ECG) and Photoplethysmogram (PPG) Features for Blood Pressure (BP) Estimation

As mentioned in Chapter 1, PTT based approaches to BP estimation have gained the most interest throughout the last few decades. Due to the ease of measurement, most studies have used PAT, which is defined as the time difference between the R-peak of the ECG and a point on distal pulse waveform such as the PPG measured at the fingertips, instead of PTT. However, since there is a considerable delay between the onset of the R-peak of the ECG and the onset of the opening of the aortic valve, PAT is not truly PTT, but contains pre-ejection period (PEP), which is defined as the time interval from the onset of ventricular depolarization to the onset of blood ejection. Though some studies promise PAT and/or PTT as the base for the future of BP measurement [19, 21, 27, 40-42], other studies show questionable results [43, 44]. In general, there have been inconsistent results about which of PAT and PTT is more suitable as BP predictor. Some studies have shown that PTT, not PAT, is related to BP through arterial compliance, and have presented experimental evidence that support this idea. For example, in 2006, Payne et al. have shown that due to the effect of PEP, changes in PAT may not be reflected with changes in BP, while PTT-based BP prediction is unaffected [75]. On the other hand, some

studies have suggested that the inclusion of PEP in PAT measurement could improve the non-invasive BP estimation [76, 77]. However, due to the limited number of subjects used in previous studies for evaluation, a comprehensive understanding of the general relationship between these predictors and BP was unavailable yet.

Many studies have attempted to find new predictors for BP estimation through extracting physiologically meaningful features from the morphology of PPG waveforms. However, most of these studies have analyzed less than 100 subjects, and all of these studies have analyzed different characteristics extracted from the morphology of the PPG waveform. To the authors' knowledge, there has not been any research that definitively confirmed how these features actually relate to BP from a large diverse database. Therefore, these indicators should be analyzed to evaluate validity of the BP predictors from a large diverse subject group.

2.1.2 Description of Surgical Biosignal Databases

As described in chapter 1, the most widely used biosignal database for the development and analysis of BP estimation models was the MIMIC database. The database comprises of biosignals measured from surgical patients enrolled in intensive care units including ECG, PPG, and arterial blood pressure (ABP) sampled at 125 Hz. All recordings are associated with a subject ID and a

recording number, but some recordings from the same subject ID may be from different subjects due to technical limitations in the organization of the database. Another fundamental limitation about the database is that the database was not aimed to be used for inter-waveform analysis as described in chapter 1. The database inconsistently contains delays or time shifts between signals due to filtering and/or unknown causes, making it unsuitable for the extraction and the analysis of traditional temporal inter-waveform features such as PAT or PTT. Considering these limitations about the database, we used the database only for the external validation of the developed BP estimation model.

For the purpose of analyzing features, training and validation of the BP estimation models, we used a part of the VitalDB data bank, which is an open access public dataset of intraoperative vital signs and biosignals collected by the Seoul National University Hospital Department of Anesthesia using the Vital Recorder program [78]. The Vital Recorder program is a free research tool for recording of time-synchronized physiological data from multiple intraoperative devices and patient monitors. The experimental setup for collecting waveform data of VitalDB is shown in Figure 2.1. The collected VitalDB data includes raw waveforms of ABP, ECG, and PPG obtained from a commercial patient monitor device (SOLAR 8000M, GE, Milwaukee, WI, USA) down-sampled to 100Hz. ECG waveform is measured using standard lead II setup, ABP waveform is measured from the radial artery, and PPG waveform is measured from the finger. All recordings are associated with a

subject ID, and each ID is matched with demographic data (e.g., age, gender, BMI, etc.), surgery & anesthesia data (e.g., surgery type, operation, type of anesthetic used, etc.), and preoperative data (e.g., presence of hypertension, blood test hemoglobin measurement, etc.).
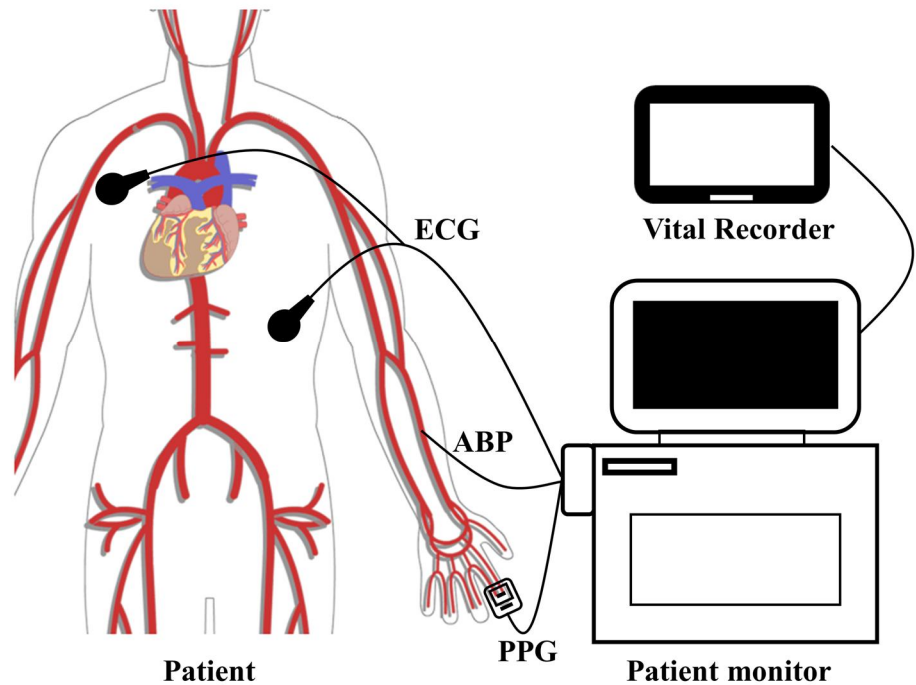
Figure 2.1 Experimental setup of VitalDB data collection protocol.

2.2 Feature Analysis

2.2.1 Data Acquisition and Data Pre-processing

The VitalDB data bank contains biosignal recordings from a total of 6388 patients undergoing various types of surgeries at the Seoul National University Hospital. Data loading, data selection, and feature extraction were performed automatically using MATLAB (MATLAB 2018b; Mathworks, Natick, MA, USA). The data used in this study were selected and pre-processed according to data selection criteria as shown in Figure 2.2.
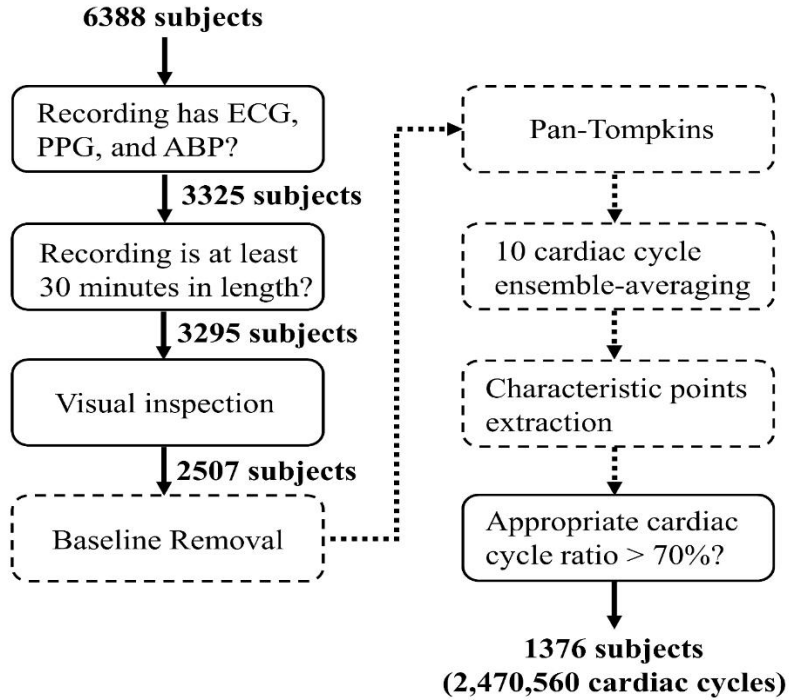
Figure 2.2 Outline of the data exclusion process for the selection of usable data from the VitalDB and data pre-processing. Solid lines correspond to the data selection criteria, and dashed lines correspond to the data pre-processing.

Since the available recordings contained segments in which the biosignals were severely distorted due to saturation and/or unknown causes generated during the surgery, several exclusion criteria were applied to remove these corrupted sections prior to analyses. The example plots of data exclusion process and data pre-processing are shown in Figure 2.3.
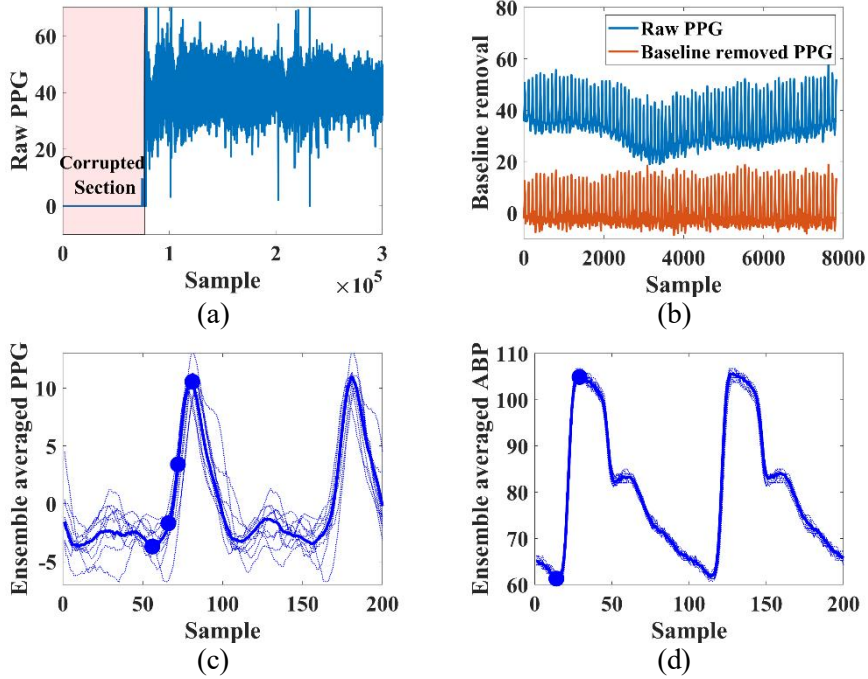
Figure 2.3 Example plots of data exclusion process and data pre-processing. (a) Example plot for visual inspection of PPG waveform with the corrupted section highlighted; (b) Example plot for baseline removal of PPG waveform; (c) Example plot of ensemble averaged PPG; (d) Example plot of ensemble averaged ABP. In (c) and (d), dotted lines denote to 10 adjacent cardiac cycles of PPG/ABP, and solid line denotes to the ensemble averaged waveform with the characteristic points of PPG/ABP labeled.

First, the recordings were checked for ECG, PPG, and ABP signals. Second, recordings less than 30 minutes were removed. Third, the recordings were visually inspected to remove some or all of the sections in which the biosignals were severely distorted due to saturation and/or unknown causes as shown in Figure 2.3(a).

Following data selection, biosignals were pre-processed to detect the characteristic points of ABP and PPG for each cardiac cycle. The detailed BP and feature extraction process is shown in Figure 2.4.
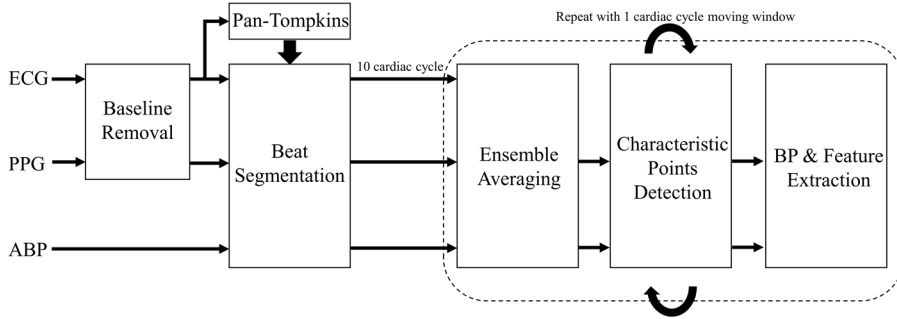
Figure 2.4 Process of BP and feature extraction from ECG, PPG, and ABP waveforms.

First, the low frequency baseline fluctuations of ECG and PPG waveforms were removed using non-linear filtering as shown in Figure 2.3(b) [79]. Then, the ECG R-peaks detected by Pan-Tompkins algorithm [80] were used to separate the waveform data into cardiac cycles for ensemble-averaging; 10 adjacent cardiac cycles of ABP and PPG were ensemble-averaged in a smoothing window manner to improve the signal-to-noise ratio (SNR) and to accentuate the waveform features as shown in Figure 2.3(c) and Figure 2.3(d). This process was repeated for the whole recording with a moving window width

of one cardiac cycle. After ensemble-averaging, the characteristic points of ABP and PPG were detected. For ABP, the peak and valley points were detected. In the case of PPG, the valleys, peaks, maximum derivatives (or the point of maximum slope), and intersecting-tangent points (or the intersecting point between the tangent lines of the maximum derivative and the diastolic minimum) [81] were detected. If the values for the all detected points in a given cardiac cycle were within pre-set time ranges (which were determined through analysis of the data set as a whole and the physiological ranges for each point), features and reference BP values were reserved for further analyses. SBP and diastolic blood pressure (DBP) were derived from the peak and the valley points of ABP, and four different PAT (PAT_V, PAT_P, PAT_{MD}, and PAT_{IT}) values were derived from the time difference between ECG R-peak and one of the characteristic points of PPG ('V' denotes the valley, 'P' denotes the peak, 'MD' denotes the maximum derivative, and 'IT' denotes the intersecting-tangent points of PPG).

Since the waveforms of ABP and PPG could be severely distorted by various artifacts, signal quality of each ensemble-averaged cardiac cycle was evaluated using the following conditions:

- Is the extracted SBP greater than 50 mmHg and less than 250 mmHg?

- Is the extracted DBP greater than 30 mmHg and less than 160 mmHg?

- Is the change in the extracted BP (SBP or DBP) during the previous 5 s interval less than 30 mmHg?

- Is the change in the extracted PATs during the previous 5 s interval less than 30 ms?

If the above conditions were satisfied, the cardiac cycle was evaluated as having high signal quality, and was determined to be appropriate for further analyses. If the ratio of the number of appropriate cardiac cycles to the total number of cardiac cycles was less than 70%, the recording was excluded as shown in Figure 2.2. Finally, 30 minutes sections in each recording were selected to adjust the number of data points per subject to a similar level for proper validation. As a result, 1376 recordings (2,470,560 cardiac cycles) were selected. The demographic characteristics of the patients and the BP characteristics of the selected data are shown in Table 2.1.

Table 2.1 Demographic and BP characteristics of the data (N=1376)

Characteristics	Subjects
Age (years)	58 ± 14 (range 8–92)
Gender (male)	720 (52%)
Height (cm)	162 ± 9
Weight (kg)	61 ± 11
BMI (kg/m^2) [a]	23 ± 3
Hypertension	484 (35%)
Diabetes	159 (12%)
# of cardiac cycles	1788 ± 289
SBP	
Mean value (mmHg)	115 ± 15
Δ value [b] (mmHg)	37 ± 19
DBP	
Mean value (mmHg)	62 ± 10
Δ value [b] (mmHg)	21 ± 11

[a]Body mass index.
[b]The difference between max and min values of each recording.

2.2.2 Feature Extraction

In order to compare the capacity between PAT and PTT to estimate BP, several PAT/PTT based BP estimation parameters were extracted from each cardiac cycle using the R-peak point of ECG, valley point of ABP, and four feature points of PPG as shown in Figure 2.5.
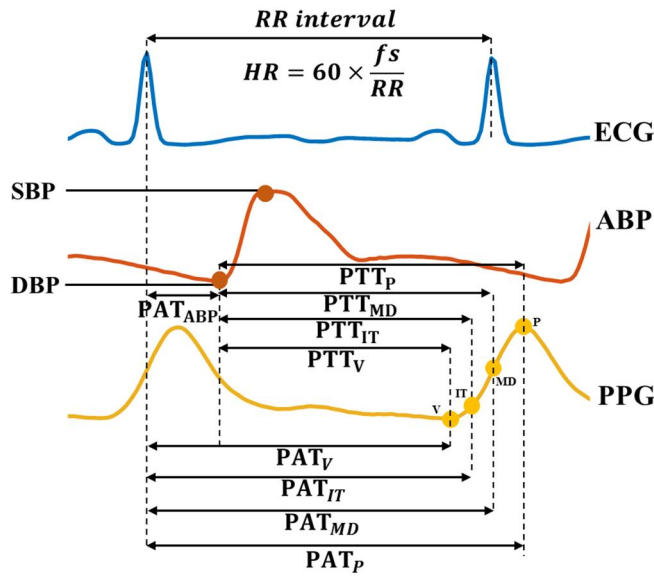
Figure 2.5 BP and PAT/PTT based features labeled on ECG, PPG, and ABP waveforms.

PAT_{ABP} was derived from the time difference between the ECG R-peak and the valley point of ABP, 4 different PAT values (PAT_V, PAT_P, PAT_{MD}, and PAT_{IT}) were derived from the time difference between the ECG R-peak and one of the characteristic points of PPG, and 4 different PTT values (PTT_V, PTT_P, PTT_{MD}, and PTT_{IT}) were derived from the time difference between the valley point of ABP and one of the characteristic points of PPG. As the goal of this study was

to validate PAT/PTT as a means of estimating BP under ubiquitous NCBPM environment, PAT_{ABP} and 4 PTT values were used only for the comparison of the validity as BP indicators with PAT, and excluded for further feature selection process, which was the process for the selection of the best feature subsets for BP estimation.

For the purpose of assessing the efficacy of PAT, HR, and various PPG morphology features as BP predictors, a total of 42 features were extracted from each cardiac cycle as shown in Figure 2.6. The definitions of the features are listed in Table 2.2.

$$HR = 60 \times \frac{fs}{RR}$$
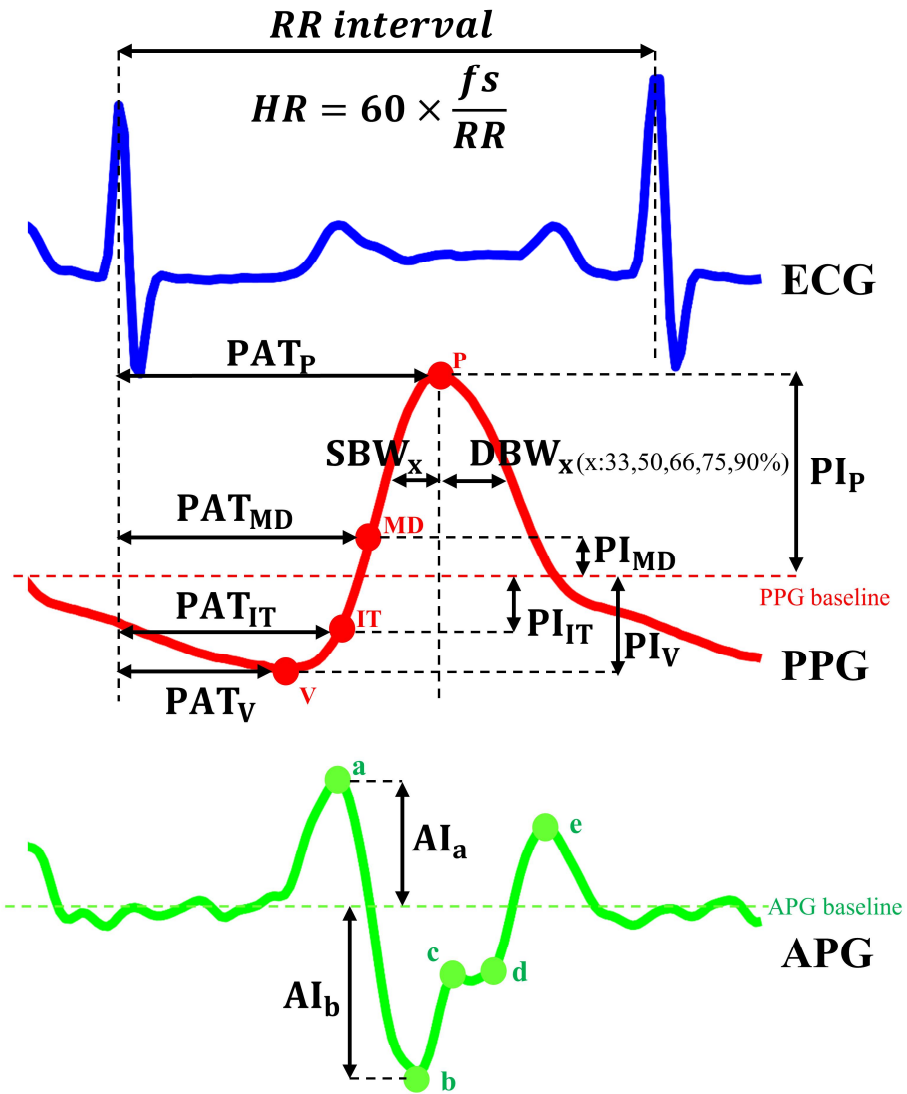
Figure 2.6 Features labeled on ECG, PPG, and APG waveforms.

Table 2.2 Definitions of the analyzed features

Index	Feature	Definition
1	PAT_V	Time delay from the R-peak of ECG to the valley point of PPG
2	PAT_P	Time delay from the R-peak of ECG to the peak point of PPG
3	PAT_{MD}	Time delay from the R-peak of ECG to the 'MD' point of PPG
4	PAT_{IT}	Time delay from the R-peak of ECG to the 'IT' point of PPG
5	HR	Time delay between two adjacent R-peaks of ECG
6	PI_V	Intensity of the valley point of PPG
7	PI_P	Intensity of the peak point of PPG
8	PI_{MD}	Intensity of the 'MD' point of PPG
9	PI_{IT}	Intensity of the 'IT' point of PPG
10	PIR_P	Ratio of PPG peak point intensity to PPG valley point intensity
11	PIR_{MD}	Ratio of PPG 'MD' point intensity to PPG valley point intensity
12	PIR_{IT}	Ratio of PPG 'IT' point intensity to PPG valley point intensity
13	CT	Time delay from the valley point of PPG to the peak point of PPG
14	AS	Ascending slope
15	PPGK	PPG characteristic value
16	SBW_{33}	
17	SBW_{50}	
18	SBW_{66}	Systolic branch width at x % of the pulse height of PPG (x: 33, 50, 66, 75, 90)
19	SBW_{75}	
20	SBW_{90}	
21	DBW_{33}	
22	DBW_{50}	
23	DBW_{66}	Diastolic branch width at x % of the pulse height of PPG (x: 33, 50, 66, 75, 90)
24	DBW_{75}	
25	DBW_{90}	
26	BW_{33}	
27	BW_{50}	
28	BW_{66}	Branch width at x % of the pulse height of PPG (x: 33, 50, 66, 75, 90)
29	BW_{75}	
30	BW_{90}	
31	BWR_{33}	
32	BWR_{50}	
33	BWR_{66}	Branch width ratio at x % of the pulse height of PPG (x: 33, 50, 66, 75, 90)
34	BWR_{75}	
35	BWR_{90}	
36	AI_a	Intensity of the a-wave of APG
37	AI_b	Intensity of the b-wave of APG
38	AIR	Ratio of APG b-wave intensity to APG a-wave intensity
39	PC1	1st principal component of the one cardiac cycle PPG
40	PC2	2nd principal component of the one cardiac cycle PPG
41	PC3	3rd principal component of the one cardiac cycle PPG
42	PC4	4th principal component of the one cardiac cycle PPG

The detailed description of PPG morphology features is as followed.

1) *Photoplethysmogram intensity ratio (PIR)*

Photoplethysmogram intensity ratio (PIR), defined as the ratio of the intensity of the peak point of PPG to the intensity of the valley point of PPG, is used as BP estimation predictor by Ding et al. [53]. According to the Beer-Lambert law, Photoplethysmogram intensity of the peak and valley point of PPG (PI_P and PI_V) can be derived as below.

$$PI_P = PI_0 \cdot e^{-\epsilon_{DC} \cdot c_{DC} \cdot d_{DC}} \cdot e^{-\alpha \cdot d_D} \tag{4}$$

$$PI_V = PI_0 \cdot e^{-\epsilon_{DC} \cdot c_{DC} \cdot d_{DC}} \cdot e^{-\alpha \cdot d_S} \tag{5}$$

where PI_0 is the incident light intensity, ε_{DC} is the absorbance coefficient, c_{DC} is the concentration, d_{DC} is the optical path of the DC component, α is the characteristic parameter, d_S and d_D are the systolic diameter and diastolic diameter, respectively. Therefore, as taking the ratio of (4) and (5), PIR is exponentially linked with arterial diameter change through the following equation:

$$PIR_P = \frac{PI_P}{PI_V} = e^{\alpha \cdot (d_S - d_D)} \tag{6}$$

Since the arterial diameter change affects total peripheral resistance, a direct influencer of BP [82], PIR_P can theoretically be used for BP estimation. In this

paper, PIR_{MD} and PIR_{IT} are additionally defined using PPG intensity of the maximum derivative or intersecting-tangent points of PPG (PI_{MD} or PI_{IT}) instead of PI_P in (6), respectively. As a result, three different PIR (PIR_P, PIR_{MD}, and PIR_{IT}) values and four different PI (PI_V, PI_P, PI_{MD}, and PI_{IT}) values are extracted.

2) Crest time (CT) and Ascending slope (AS)

Crest time (CT), defined as the time delay from the valley point to the peak point of the PPG waveform is known to be a useful feature for cardiovascular disease classification [54]. Ascending slope (AS) was previously reported as the rate of wave front sloping for BP estimation [57]. In this study, CT and AS was calculated as below.

$$CT = PAT_P - PAT_V \tag{7}$$

$$AS = \frac{PI_P - PI_V}{PAT_P - PAT_V} \tag{8}$$

3) PPGK

PPGK, also called PPG characteristic value or K value, was previously reported to be related to total peripheral resistance and blood viscosity [56]. PPGK is based on the change of PPG area and defined as below.

$$PPGK = \frac{P_m - PI_V}{PI_P - PI_V} \qquad (9)$$

where P_m is the average value of one cardiac cycle of PPG waveform.

4) Branch width (BW) based features

Awad et al. previously reported that pulse width at half height of a PPG waveform is related to total peripheral resistance [55]. Following this study, in order to extract as much information as possible, Kurylyak *et al.* calculated the widths at 25%, 33% and 75% of the pulse height and extracted separate values for the systolic part and for the diastolic part, and for the ratio between these values [83]. In this paper, systolic branch width (SBW) is defined as the systolic part of the pulse width, diastolic branch width (DBW) is defined as the diastolic part of the pulse width as shown in Figure 2.6. Branch width (BW) is defined as the sum of SBW and DBW, and branch width ratio (BWR) is defined as the ratio of DBW to SBW. BW, SBW, DBW, and BWR are calculated at 33%, 50%, 66%, 75%, and 90% height of the beat respectively.

5) Acceleration plethysmogram (APG) features

The second derivative of PPG waveform, also called the acceleration plethysmogram (APG) is an indicator of the acceleration of the pulse through an artery. The waveform of the APG includes five waves, namely a-wave to e-wave as shown in Figure 2.6. The ratios of the height of the each wave to that

of the a-wave are commonly used as characteristic waveform features of APG [58]. APG intensity ratio (AIR), defined as the ratio of the APG intensity of the b-wave (AI_b) to the APG intensity of the a-wave (AI_a), is reported to reflect arterial stiffness and distensibility of the peripheral artery [84]. The c-wave to e-wave of APG are usually used to detect the dicrotic notch and diastolic peak point of PPG waveform [58]. However, a dicrotic notch is usually only seen in subjects with healthy compliant arteries [85]. According to a previous study, the higher harmonic frequency components of PPG diminish with age, consistent with the loss of the dicrotic notch features in older subjects [86]. Therefore, in this study, features related to the dicrotic notch such as c-wave to e-wave in APG waveform, augmentation index [84], and large artery stiffness index [87] were excluded from further analyses in order to develop a generalized BP estimation model for heterogeneous subjects. As a result, three features (AIR, AI_a, and AI_b) are extracted from the APG waveform.

6) Principal component analysis (PCA) features

All of the above-mentioned features are based on assumptions that these characteristic points of the PPG are potentially meaningful in terms of physiology. On the other hand, principal component analysis (PCA) features are a representation of the whole PPG waveform shape and timing. This approach is presented as a "whole-based feature" in a previous study [59]. In this paper, PCA features were extracted as followed. First, the PPG waveform

in each cardiac cycle is re-sampled to 100 points equally. Second, each cardiac cycle of PPG is normalized by dividing by the maximum value of the waveform (the offset was previously removed during pre-processing steps). Finally, PCA is used to aggregate and analyze each pre-processed cardiac cycles of PPG for each subject. In other words, one cardiac cycle of PPG is treated as a 100-dimensional data point. Top 4 principal components (PC1, PC2, PC3, and PC4) were chosen among results of the PCA for further analyses. The whole process of PCA features extraction and the example plot of input PPG data for PCA are shown in Figure 2.7.
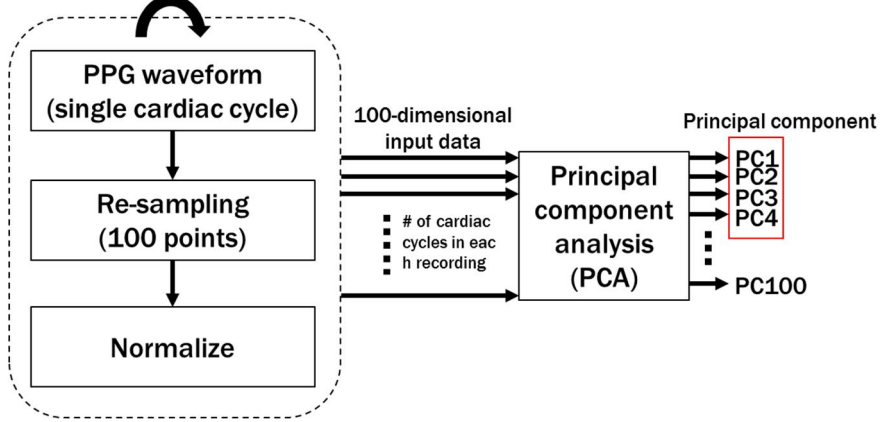
(a)
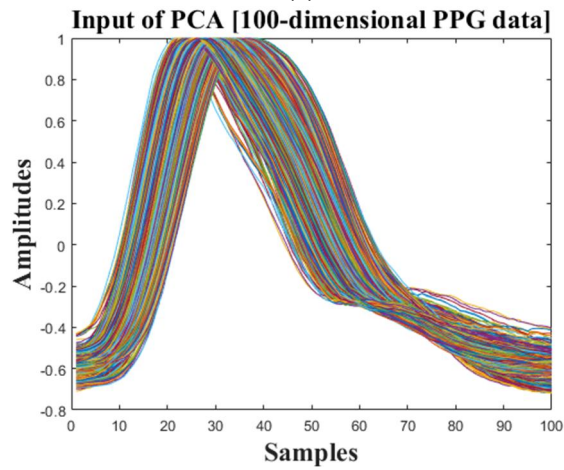
(b)

Figure 2.7 Process and example plot of PCA features extraction. (a) The whole process of PCA features extraction; (b) Example plot of input PPG data for PCA.

2.2.3 Feature Selection

Feature selection is a preprocessing technique which provides an understanding of the underlying structure and characteristics of the data through the analysis of the features. In general, the aims of feature selection process are: 1) to eliminate irrelevant and redundant features to reduce the dimensionality of the data; and 2) to gain a better understanding of the features and their relationship to the response variables (in our case, BP) [88]. However, these two goals are often at odds with each other. A feature selection method that is good for purpose 1) isn't necessarily good for purpose 2) and vice versa. If a feature selection method is useful to build a good predictor subset to reduce the dimensionality of the data, a resultant subset might exclude many redundant, but relevant features. Conversely, if a feature selection method which is oriented to find or rank all potentially relevant features, it could reliably assess the statistical significance of the relevance of the features. For example, lasso regression method, which is a linear regression model with L1 regularization method [89], is very useful when reducing the number of features is required, but not for data interpretation since it picks out the top performing features, while forcing other features to be close to zero even if they have a strong relationship with the output variable. However, ridge regression method, which is a linear regression model with L2 regularization [90], is useful for feature

interpretation since predictive features will get non-zero coefficients even though they have feature redundancies.

As the purpose of our study was to evaluate the validity of diverse PPG morphology features as BP predictors, we have applied several feature selection methods which were more suitable for purpose (2) to the extracted features in order to assess the statistical significance of the "relevance" of the features. Feature "redundancy" was not considered since the fundamental purpose of feature selection in this study was not to reduce the dimensionality of the features. Furthermore, noise reduction and better estimation performance might be obtained by adding variables that were presumed to be redundant [88].

Before performing feature selection process, the mean value of BP was subtracted from the BP values and the mean value of each feature was subtracted from the feature values in a given recording for the purpose of calibration, and then these values obtained from 1376 subjects were analyzed. As a result, a total of 2,470,560 pairs of BP and features were analyzed for feature interpretation.

All feature selection processes were performed using Python (version 3.6.3) and Scikit-learn library (version 0.19.1). As shown in Figure 2.8, feature selection methods were categorized into filter methods, wrapper methods, and embedded methods [88]. A detailed description of each method is as followed.
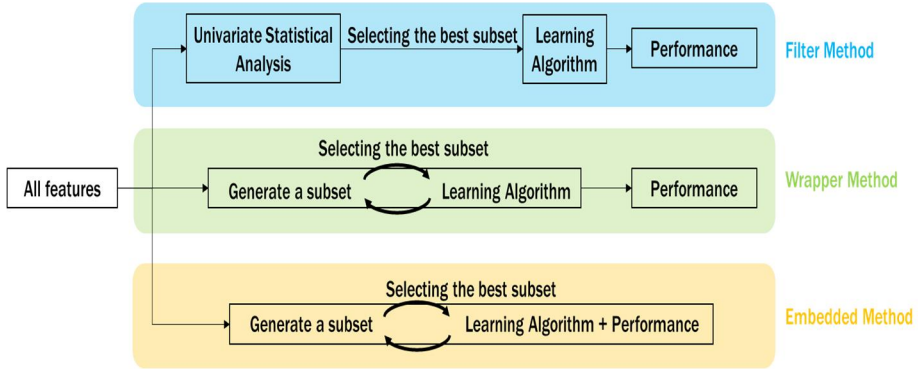
Figure 2.8 Three types of feature selection.

1) Filter methods

Filter methods are based on univariate statistical techniques to evaluate the strength of the relationship of each feature and the response variable [91]. These methods are simple to run and they give fast and efficient results on execution. In this study, Pearson correlation coefficient and mutual information (MI) were analyzed.

Pearson correlation coefficient is one of the simplest methods for understanding a feature's relation to the response variable by measuring linear correlation between two variables. It is fast and easy to calculate and is often the first thing to be run on the data. In this study, Pearson correlation coefficient was calculated between each feature and BP as followed.

$$\rho(\mathbf{X}, \mathbf{Y}) = \frac{\mathbf{E}((\mathbf{X} - \boldsymbol{\mu_X})(\mathbf{Y} - \boldsymbol{\mu_Y}))}{\boldsymbol{\sigma_X}\boldsymbol{\sigma_Y}} \qquad (10)$$

where σ_X and σ_Y are the standard deviations of X and Y, μ_X and μ_Y are the means of X and Y, and E is the expected value.

Although Pearson correlation is a useful method due to its low computational cost, it has the obvious drawback as a feature selection method that it only captures linear dependency. MI is a more robust method for correlation measure, which measures mutual dependence between variables [92]. Since the function relies on nonparametric methods based on entropy estimation from k-nearest neighbors distances, it is able to find the non-linear relationship between variables [92].

2) Wrapper methods

Wrapper methods incorporate learning algorithm in the process of feature selection [91]. It ranks features based on the regression performance. One of the representative techniques in wrapper methods is recursive feature elimination (RFE). The high level idea of RFE is to iteratively construct an estimation model that assigns weights to features (e.g. the coefficients or the weights of a learning algorithm) and remove features whose absolute weights are the smallest [93]. The procedure is recursively repeated until the pre-defined number of features remain. In this study, RFE with linear support vector machine (SVM) regression model was performed. Varying the hyper-parameters of SVM such as epsilon or regularization parameter did not lead to significant difference in the RFE results. Therefore, epsilon was set to 0, and regularization parameter was set to 1. The number of features to select in RFE was set to 5. The algorithm of RFE used in this study is as shown in Figure 2.9.
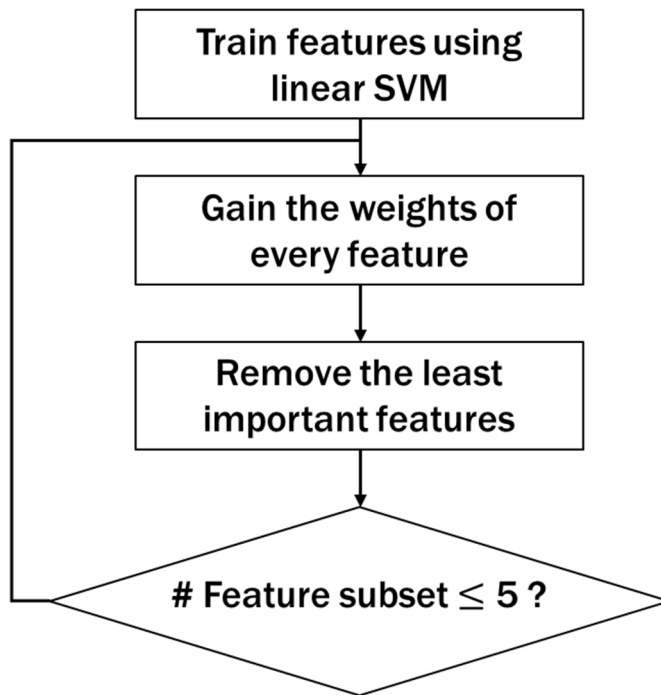
Figure 2.9 The algorithm of RFE.

3) Embedded methods

Similar to wrapper methods, embedded methods are also used to optimize the performance of a learning algorithm. The difference to wrapper methods is that the feature selection is performed as a part of the training process, and the method of selecting optimal feature subset is specific for the given regression methods [91]. Among the embedded methods, ridge regression, randomized lasso regression, and random forest's impurity-based ranking were performed in this study.

Ridge regression is a linear regression model with L2 regularization method [90]. The effect of L2 regularization is that models are much more stable,

meaning that coefficient values of regression model do not fluctuate on small changes in the data, making the model more useful for feature interpretation than pure linear regression or lasso regression, which used L1 regularization method [89]. Ridge regression has one hyper-parameter called α, which determines the amount of regularization. In this study, α is tuned using the grid search method.

Randomized lasso regression is a novel method for feature selection, based on subsampling in combination with lasso regression model [89]. This method is based on the idea to apply a feature selection algorithm on different subsets of data and with different subsets of features. After repeating the procedure a number of times, the results of feature selection are aggregated. By this method, randomized lasso is more suitable for feature interpretation, since correlated features tend to get similar coefficients, unlike the pure lasso regression. Similar to ridge regression, the hyper-parameter called α in this method is tuned using the grid search method.

Random forest for regression is an ensemble learning method that combines a multitude of decision trees to output the mean prediction of the individual trees [94]. It is one of the most popular machine learning algorithms due to its relatively good accuracy, robustness and ease of use. Another advantage of random forest is that it also provides the relative importance of each feature. The importance of each feature is calculated by looking at how much the decision tree nodes that use that feature reduce impurity on average. The

detailed description of constructing random forest model will be discussed in section 2.3.2.

Finally, a total of six feature selection methods (Pearson correlation coefficient, MI, RFE, ridge regression, randomized lasso regression, and random forest's impurity-based ranking) were applied in this study in order to reliably assess the statistical significance of the relevance of the features to BP. The feature importance scores calculated by using each of the methods were normalized to a scale between 0 and 1. Then, the mean value of feature importance scores for each feature were analyzed to gain an interpretation of the features and to determine the best BP estimation predictors amongst all the features. The whole process of feature selection is shown in Figure 2.10.
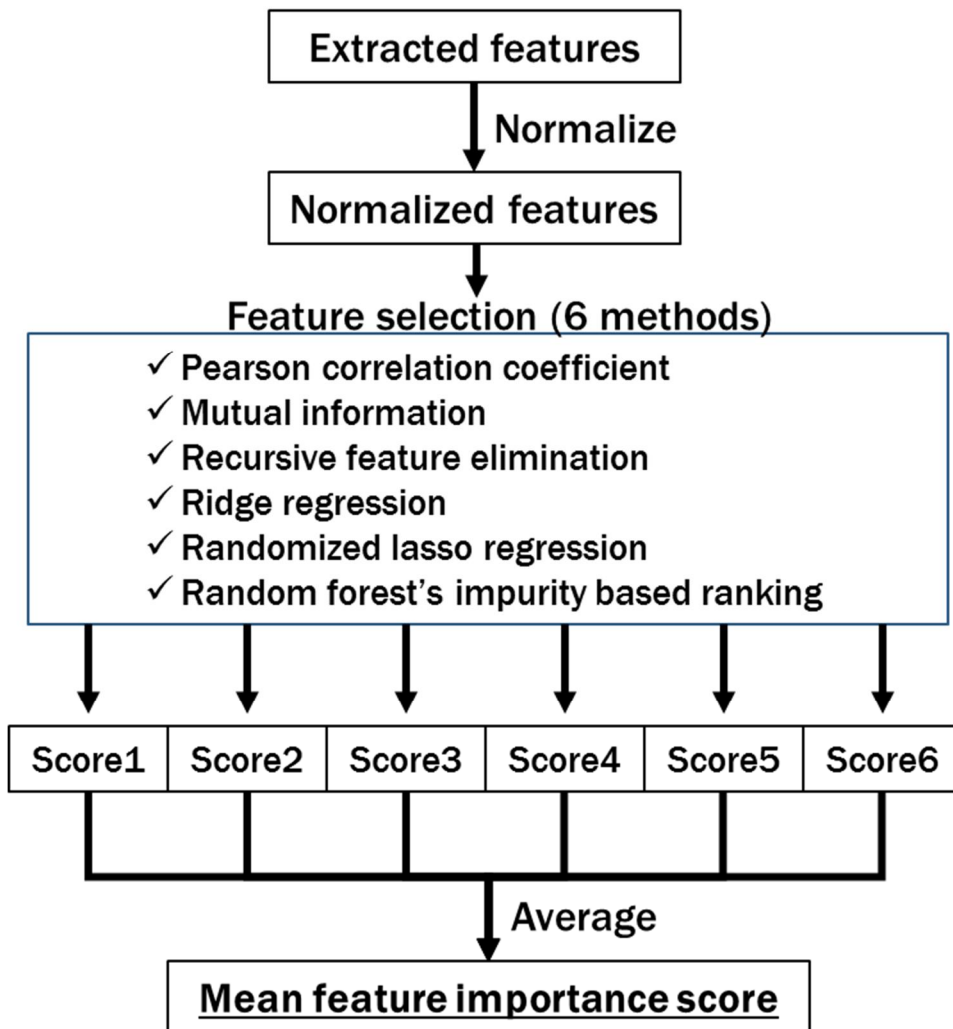
Figure 2.10 Outline of the feature selection process.

For the purpose of validating the feature selection without considering feature redundancy, the result was compared with two well-known feature selection algorithms introduced in a prior research [95]. The first is the MaxRel algorithm that maximizes the average of the mutual information values between the response variable and each feature of the subset, and the second is the

minimal-redundancy-maximal-relevance (mRMR) algorithm which combines MaxRel algorithm and min-redundancy criterion that minimizes the dependencies between features of the subset.

2.3 Construction of the BP Estimation Models

2.3.1 Frequency Component Separation

Some previous studies have suggested that BP estimation features such as PAT could track only certain frequency components of BP variation. Chen *et al.* reported that lower frequency component of PAT was not well correlated to SBP [19]. Therefore, they combined the high frequency component of PAT and used intermittent calibration to adjust for low frequency fluctuations of BP. Ding *et al.* also suggested that PAT could track BP in high frequency range well, but was inadequate to follow the low frequency variations in BP [49]. They proposed PIR as an indicator that could track BP in the low frequency range. These studies showed that the linear relationship between BP and certain predictors can be more apparent when BP and features are separated based on frequency. Therefore, estimation performance may be improved by separating BP and feature variations into low frequency components (LFC) and high frequency components (HFC), and modeling each separately.

In order to verify this hypothesis, extracted BP and features were separated into LFC and HFC. First, since the BP and features were extracted on beat-by-beat basis, they were re-sampled to a sampling rate of 1 Hz using cubic spline interpolation (i.e., resampled in the time domain to be 1 cardiac cycle per second). Then, LFC of BP and features were obtained by filtering using a 1st

order low-pass Butterworth digital filter. HFC of BP and features were obtained by subtracting the LFC of BP and features from the raw BP and features. The cutoff frequency of the low-pass filter was set at 0.004 Hz, referring to a previous study showing a linear relationship between SBP and PAT between 0.00053 Hz to 0.004 Hz [19]. Figure 2.11 shows the example plots of separating SBP and PAT_{IT} into their LFC and HFC. The optimal cutoff frequency was determined by comparing the performance of the BP estimation model constructed by linear regression algorithm for each cutoff frequency.
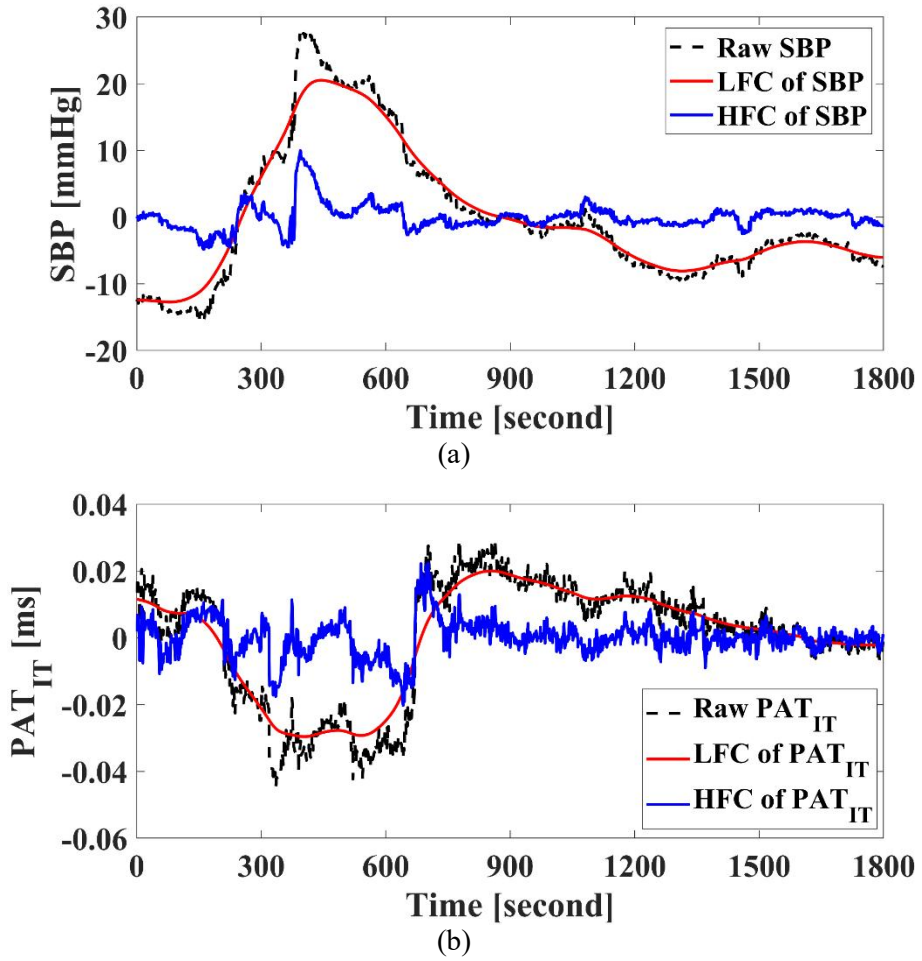
Figure 2.11 Example plots of separating SBP and PAT$_{IT}$ into LFC and HFC. (a) Example plot of raw SBP (dotted black line), LFC of SBP (solid red line), and HFC of SBP (solid blue line) from one representative subject; (b) Example plot of raw PAT$_{IT}$ (dotted black line), LFC of PAT$_{IT}$ (solid red line), and HFC of PAT$_{IT}$ (solid blue line) from one representative subject. Raw SBP and PAT$_{IT}$ are the calibrated values.

2.3.2 Modelling Algorithms

BP estimation models based on the selected features using several modeling algorithms were constructed and evaluated. The LFC and HFC of BP were modelled separately. That is, the LFC of BP was estimated by the LFC of the features, and the HFC of BP was estimated by the HFC of the features. In order to calibrate the model to each subject, the mean value of BP was subtracted from the BP values and the mean value of each feature was subtracted from the feature values in a given recording prior to modeling. Then, the mean BP was added back to the BP estimate model output for each subject.

The entire dataset consisting of 1376 subjects was randomly divided into two sets in 7:3 ratio; 963 recordings were used to train BP estimation model and 413 recordings were used for validation accounting for a total of 741,690 cardiac cycles. The two-sample t-test between the training and the validation dataset showed no statistically significant differences in age, gender, height, weight, BMI, SBP values, and DBP values between the two groups. The modeling algorithms used in this study included linear regression, random forest, artificial neural network, and recurrent neural network. The detailed description of these algorithms is as followed.

1) Linear regression (LR)

As a baseline machine learning model, linear regression (LR) is the most widely used regression method that models the linear relationship between a dependent variable and explanatory variables to come up with a best fit linear equation from observed data. In this study, dependent variable is BP and explanatory variables are the selected features. LR model was trained using a MATLAB script.

2) Random forest (RF)

Due to the size of the training dataset in this study (more than 1 million cardiac cycles), a method called "Extremely Randomized Trees", which is computationally less expensive than the typical random forest method was used [96]. Parameters such as the number of trees, the maximum number of leaf nodes, and the minimum number of samples required to be at a leaf node were tuned using the grid search method. The RF model in this study consisted of 500 trees with the maximum 10,000 leaf nodes, and the minimum 100 samples required to be at a leaf node. The training of RF was done using Python and Scikit-learn library.

3) Artificial neural network (ANN)

Artificial neural network (ANN) is the most basic of neural network architecture. It consists of input and output layers, as well as hidden layers

consisting of units that perform mathematical transforms for adding non-linearity. Parameters of ANN such as the number of hidden layers, the number of hidden nodes, and the kinds of activation function in hidden nodes were chosen after considering multiple different combinations. The network topology in this study consisted of an input layer, one hidden layer with 100 nodes using tanh function as an activation function, and one node for SBP or DBP prediction in the output layer as shown in Figure 2.12(a). Mean Squared Error (MSE) was used as a cost function. To optimize the network, an ADAM optimizer with initial learning rate of 0.001 was used. The training of ANN was done using Python and Tensorflow (version 1.12.0).

4) Recurrent neural network (RNN)

Recurrent neural network (RNN) is a deep neural network that is apt for analyzing and predicting sequential information. In a traditional ANN architecture, the network takes the input as features at a certain time and predict the outcome (in our case, BP) at the same time. However, in the case of RNN, since the network has a recurring connection to itself at consecutive time points, the features from a previous time step can influence the prediction of BP at a future time step [97]. Since BP dynamics are temporally dependent in nature, RNN can be a better modelling algorithm as compared to ANN. In this study, a RNN model was constructed in a many-to-many fashion consisting of bidirectional long short-term memory (LSTM) cells [98, 99]. Bidirectional

RNN connects two hidden layers of opposite directions to the same output in order to get information from the future states as well. Similar to ANN, the architecture of RNN developed in this study was chosen after considering multiple different architectures. The chosen network consisted of 2 hidden layers with 40 LSTM cells in each layer, and 250 time steps as shown in Figure 2.12(b). To optimize the network, an ADAM optimizer with initial learning rate of 0.01 was used. The training of RNN was done using Python and Tensorflow.
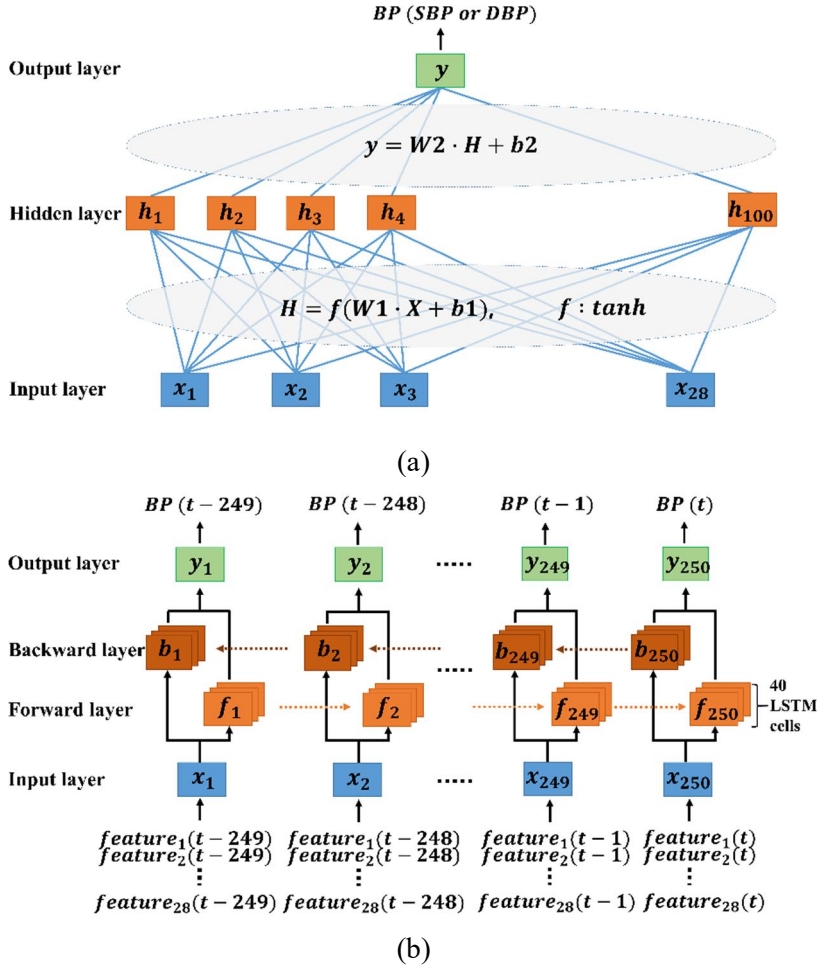
Figure 2.12 The architectures of the ANN and RNN used in this study. (a) The architecture of the ANN; (b) The architecture of the RNN.

The performance of the constructed BP models was evaluated against three international standards. First, mean error (ME) and standard deviation of the error (SDE) were calculated to validate the models against the Association for the Advancement of Medical Instrumentation (AAMI) standards, which requires ME and SDE values lower than 5 and 8 mmHg [100]. Second, the cumulative error percentages within 5, 10, and 15 mmHg were calculated to evaluate the models against the British Hypertension Society (BHS) BP monitor

51

standards, which grades devices based on their cumulative error percentages under three different thresholds [101]. Finally, the mean absolute difference (MAD) was calculated to evaluate the models in accordance with the latest standard for wearable and cuffless BP monitoring devices published by the IEEE Engineering in Medicine and Biology Society (IEEE Standard 1708) [102]. All performance measures were calculated between the estimated BP (i.e., the sum of the outputs of the LFC estimation model and the HFC estimation model) and the reference BP. The definitions of ME, SDE, and MAD are as followed.

$$\mathbf{ME} = \frac{\sum_{i=1}^{n}(p_i - y_i)}{n} \tag{11}$$

$$\mathbf{SDE} = \sqrt{\frac{\sum_{i=1}^{n}\{(p_i - y_i) - ME\}^2}{n-1}} \tag{12}$$

$$\mathbf{MAD} = \frac{\sum_{i=1}^{n}|p_i - y_i|}{n} \tag{13}$$

where p_i denotes the estimated BP value, y_i denotes the reference BP value, and n is the data size.

2.3.3 Summary of Training and Validation

A summary of BP estimation model training and validation is shown in Figure 2.13.
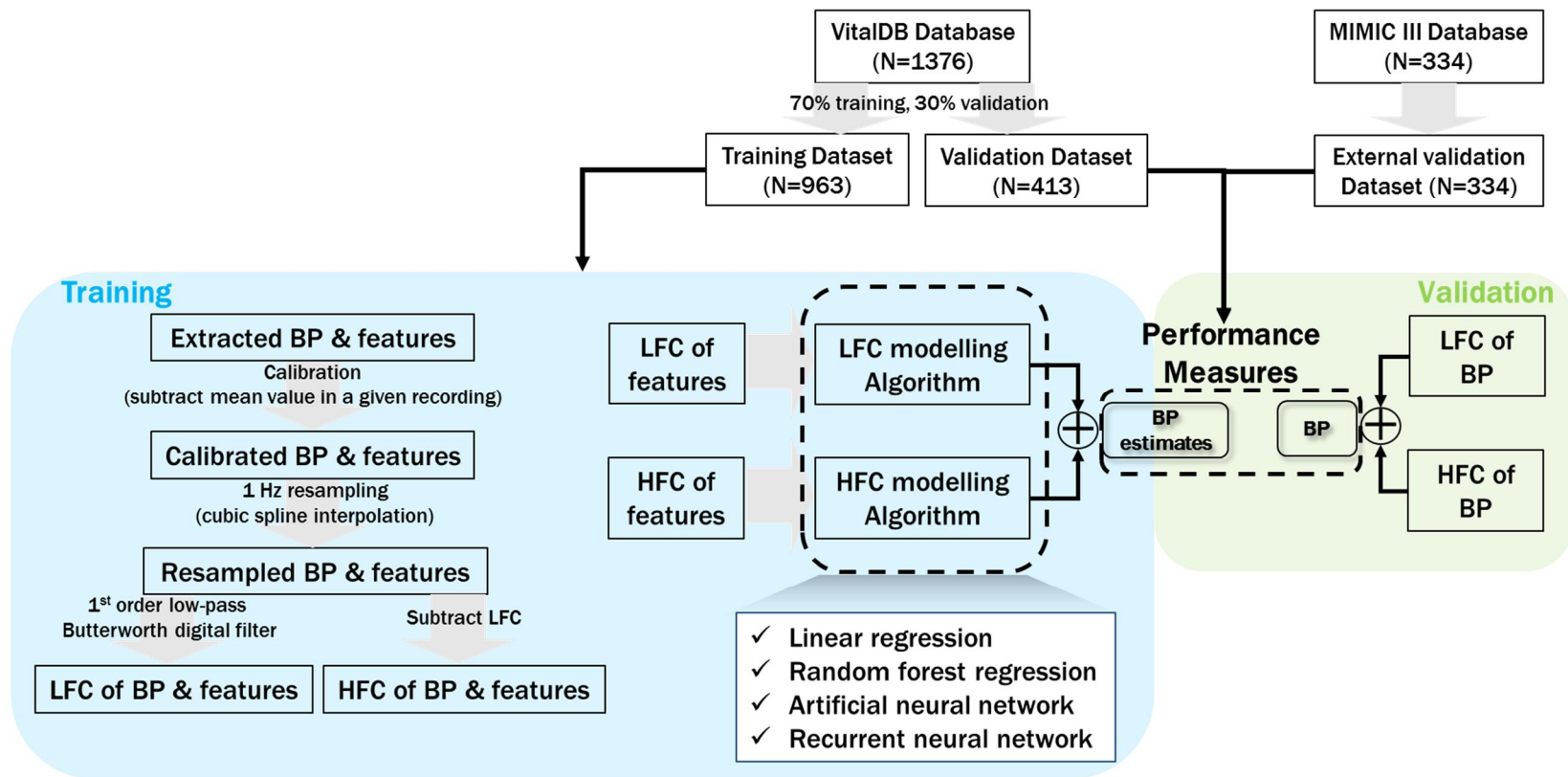
Figure 2.13 BP estimation model training and validation outline.

2.4 Results and Discussion

2.4.1 Feature Analysis

2.4.1.1 Pulse Arrival Time versus Pulse Transit Time

The mean and standard deviation of the Pearson correlation coefficients between the two BP values (i.e., SBP and DBP) and the nine PAT/PTT based features (i.e., PAT_{ABP}, four PATs, and four PTTs) are shown in Table 2.3.

Table 2.3 Correlation analysis result of PAT/PTT based features

	PAT_{ABP}	PAT_V	PAT_P	PAT_{MD}	PAT_{IT}	PTT_V	PTT_P	PTT_{MD}	PTT_{IT}
SBP	-0.44±0.34	-0.25±0.39	-0.20±0.42	-0.31±0.36	-0.34±0.37	-0.05±0.38	0.01±0.40	-0.09±0.35	-0.11±0.36
DBP	-0.34±0.37	-0.20±0.39	-0.16±0.41	-0.25±0.36	-0.28±0.37	-0.06±0.37	-0.00±0.39	-0.09±0.35	-0.11±0.36

Among the features, PAT_{ABP} showed the highest mean correlation to BP with -0.44 for SBP and -0.34 for DBP. Among the four PATs derived between ECG and PPG, PAT_{IT} showed the highest mean correlation to BP with -0.34 for SBP and -0.28 for DBP. In the case of PTT, PTT_{IT} showed the highest mean correlation to BP, but showed very weak mean correlation with -0.11 for SBP and -0.11 for DBP. The box plots of the correlation coefficients between two BP values and three features (PAT_{ABP}, PAT_{IT}, and PTT_{IT}) are shown in Figure 2.14.
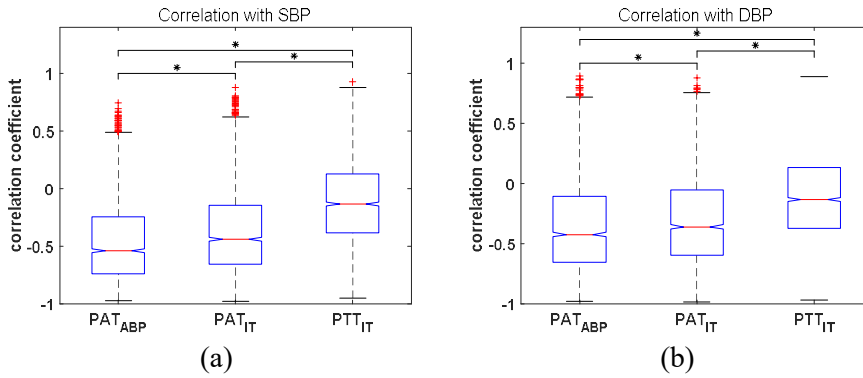
Figure 2.14 Box plots of the Pearson correlation coefficients between BP values and PAT/PTT values across 1376 subjects. On each box, the central mark indicates the median, and the bottom and top edges of the box indicate the 25th and 75th percentiles, respectively. The whiskers extend to the most extreme data points not considered outliers, and the outliers are labeled with the '+' symbol. (a) Box plot for SBP; (b) Box plot for DBP. *P<0.001 using the paired t-test.

Contrary to prior studies [75, 76, 103], PAT was found to be a superior predictor of BP as compared to PTT. Many previous studies have shown that PTT, not PAT, is related to BP through arterial compliance, and have presented experimental evidence that support this idea. However, with regards to the development of a practical mobile NCBPM, PTT is often measured as the time difference between two PPG points (due to the small size and the low cost of PPG sensors), and this results in PTT that is derived from pulse propagation paths composed of both large arteries and peripheral arteries.

The smooth muscle interactions in peripheral arteries invalidate the assumptions of the arterial compliance model of BP [39], and in contrast, disregarding the effect of PEP, PAT derived between ECG and ABP is derived from paths composing of large arteries that satisfy the above assumptions. As seen in Figure 2.1, the pulse propagation path for the measured PTT is between

the radial artery and the peripheral arteries of the index finger, while the pulse propagation path for the measured PAT includes the path from the heart to the radial artery as well. Overall, the relative distance of the propagation path unaffected by smooth muscle interactions may be much greater for PAT as compared to PTT, and this is reflected on the correlation results shown in Table 2.3. The correlation values between BP and PAT are similar to the correlation values between BP and PAT_{ABP}, while the correlation values between BP and PTT are significantly lower. This discrepancy indicates that pulse propagation timing mainly through large elastic arteries (i.e., 4 PATs or PAT_{ABP}) can be used for BP estimation, but increasing ratio of peripheral arteries in pulse propagation path (i.e., 4 PTTs) leads to the breakdown of the arterial compliance BP model.

Although previous studies have theorized that smooth muscle interactions in peripheral arteries would negatively affect PAT or PTT as predictors of BP, quantitative or qualitative analysis on this concept in regards to NCBPM was unavailable. These results provide evidence for the negative effect of smooth muscle interactions on arterial compliance model-based estimation of BP, and provide insight on the potential modalities capable of measuring parameters related to BP. The measurement of PTT or PAT in large arteries using invasive means is in agreement with theory and may be ideal for BP estimation (as seen in the difference between correlation coefficients between BP and PAT_{ABP} or 4 PATs), but PTT derived from peripheral arteries using non-invasive means such

as two PPGs are not adequate surrogates for BP estimation. To avoid the aforementioned issue, if two peripheral points of the body are to be used for PTT measurement for NCBPM, alternatives to PPG, such as mechanical pulse detection, should be used. Additionally, since the correlation values for PAT_{ABP} and PAT_{IT} are similar, PAT derived from ECG R-peak and PPG may still have value in BP estimation as long as the distal point of pulse detection has long enough pulse propagation path through large arteries. With considerations to the potential effect of PEP as described in [75, 103], the ideal solution for NCBPM would involve a system which measures PTT from the aortic opening to a distal point using non-photoplethysmographic means, such as a system composing of seismocardiogram (SCG) and mechanical pulse detection at the wrist.

2.4.1.2 Feature Selection

The results of feature selection processes analyzing a total of 2,470,560 pairs of SBP and the extracted 42 features are shown in Table 2.4 and Figure 2.15.

Table 2.4 Feature importance scores of top 28 ranked features

Rank	Feature	Feature importance score (feature selection analyses with SBP)						
		Pearson	MI	RF	RFE	Ridge	R-lasso	Mean
1	PPGK	**1.00**[a]	**0.93**[a]	**1.00**[a]	0.81	**0.83**[a]	**0.89**[a]	**0.91**[a]
2	PIR_P	**0.98**[a]	**0.95**[a]	**0.90**[a]	0.84	**0.74**[a]	**0.97**[a]	**0.90**[a]
3	HR	0.43	**1.00**[a]	**0.90**[a]	**1.00**[a]	**1.00**[a]	**1.00**[a]	**0.89**[a]
4	PAT_{IT}	**0.65**[a]	0.74	**0.98**[a]	**1.00**[a]	0.59	**0.91**[a]	**0.81**[a]
5	BW_{66}	**0.64**[a]	**0.88**[a]	0.33	**1.00**[a]	0.59	0.61	**0.68**[a]
6	BW_{75}	**0.63**[a]	**0.89**[a]	0.45	0.65	0.22	**0.89**[a]	0.62
7	AI_b	0.26	0.55	0.10	0.76	0.44	0.49	0.43
8	PI_P	0.22	0.66	0.11	0.78	0.55	0.25	0.43
9	SBW_{66}	0.23	0.30	0.06	0.97	**0.81**[a]	0.09	0.41
10	BWR_{50}	0.09	0.34	0.03	**1.00**[a]	**1.00**[a]	0.00	0.41
11	PAT_V	0.32	0.51	0.18	0.89	0.06	0.45	0.40
12	SBW_{50}	0.20	0.32	0.06	**1.00**[a]	0.74	0.00	0.39
13	DBW_{50}	0.34	0.60	0.07	0.86	0.47	0.01	0.39
14	PAT_{MD}	0.54	0.52	**0.57**[a]	0.11	0.06	0.50	0.38
15	BW_{90}	0.44	0.78	0.21	0.38	0.03	0.36	0.37
16	DBW_{90}	0.36	0.51	0.10	0.92	0.23	0.03	0.36
17	PC2	0.21	0.31	0.11	0.95	0.41	0.03	0.34
18	BW_{50}	0.48	0.82	0.13	0.46	0.03	0.09	0.34
19	AS	0.14	0.41	0.09	0.68	0.40	0.09	0.30
20	DBW_{33}	0.17	0.62	0.04	0.49	0.31	0.00	0.27
21	SBW_{75}	0.22	0.28	0.04	0.73	0.29	0.04	0.27
22	PAT_P	0.14	0.52	0.16	0.51	0.13	0.12	0.26
23	DBW_{75}	0.49	0.66	0.21	0.05	0.00	0.09	0.25
24	BWR_{66}	0.19	0.39	0.02	0.70	0.20	0.00	0.25
25	DBW_{66}	0.48	0.67	0.13	0.14	0.06	0.03	0.25
26	PI_V	0.03	0.55	0.06	0.62	0.26	0.00	0.25
27	CT	0.09	0.40	0.07	0.59	0.27	0.00	0.24
28	PC1	0.01	0.28	0.18	0.57	0.11	0.00	0.19

[a]Top 5 features in each feature selection method.
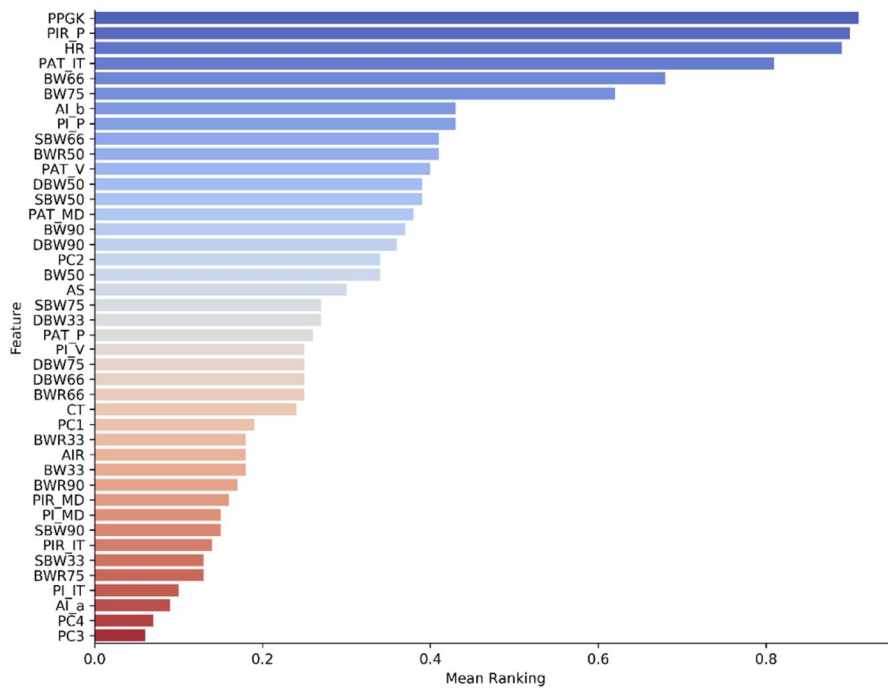
Figure 2.15 Bar plots of the mean feature importance scores of 42 features across 1376 subjects.

Although the top features ranked by different feature selection methods vary as shown in Table 2.4, PPGK, PIR_P, HR, PAT_{IT}, BW_{66}, and BW_{75} rank high across almost all methods. Among them, PPGK has the highest feature importance score with a mean value of 0.91. The absolute Pearson correlation coefficient value of PPGK was 0.49 for SBP, and 0.48 for DBP. Among the four PAT values, PAT_{IT} showed the highest mean feature importance score with the highest Pearson correlation, consistent with the findings of the previous study [104]. Among the PPG morphology features, PPGK and PIR_P along with HR showed higher mean feature importance score when compared to PAT_{IT}. Similar results were found on the same feature selection analyses with DBP.

When comparing SDE and MAD values calculated from the linear regression models constructed by sequentially adding features in order of highest mean feature importance score, there were no significant differences between the model using only 28 features and one using all features. Therefore, PPGK, PIR_P, HR, PAT_{IT}, BW_{66}, BW_{75}, AI_b, PI_P, SBW_{66}, BWR_{50}, PAT_V, SBW_{50}, DBW_{50}, PAT_{MD}, BW_{90}, DBW_{90}, PC2, BW_{50}, AS, DBW_{33}, SBW_{75}, PAT_P, DBW_{75}, BWR_{66}, DBW_{66}, PI_V, CT, and PC1 were selected as the BP estimation predictors (totaling 28 features) for further analyses.

In order to validate the feature selection results, the proposed feature selection algorithm in this study without considering feature redundancy was compared with the MaxRel algorithm and the mRMR algorithm. The three methods (proposed, MaxRel, and mRMR) were used to select 28 sequential feature sets and computed the respective SDE values using linear regression. As shown in Figure 2.16, for most feature numbers $\in \{1, 28\}$, smaller SDE values on proposed feature sets were obtained.
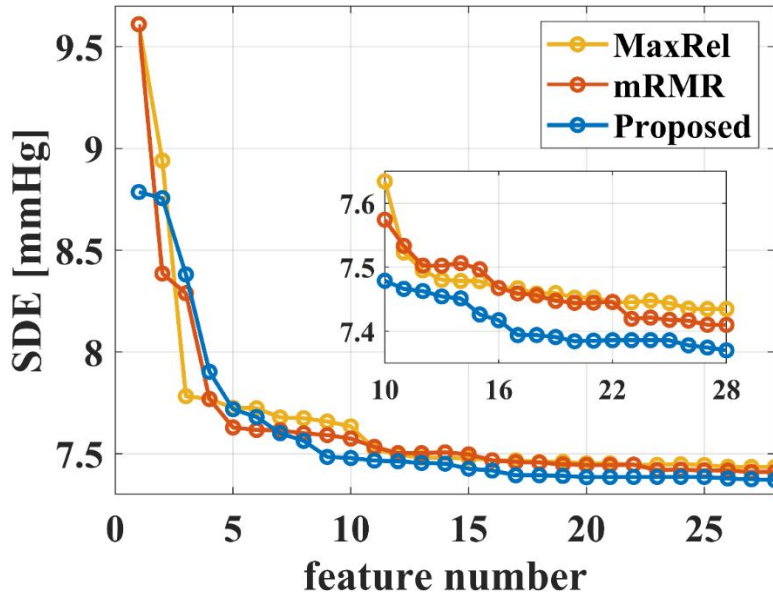
Figure 2.16 Comparison of estimation performance of the proposed, MaxRel, and mRMR algorithms.

This is the first study to use a large heterogeneous dataset to validate the potential of a diverse PPG morphology features as predictors of BP comprehensively. The key finding of the feature selection result was that 28 features including several PPG morphology features and PAT were determined as suitable BP predictors, in particular two PPG morphology features (PPGK and PIR_P) outperformed PAT, which has been conventionally seen as the best non-invasive indicator of BP. Similar results were found in a prior study analyzing several PPG morphology features using a genetic algorithm based feature selection method, although the number of subjects in the study was less than 100 [48].

Total peripheral resistance refers to the resistance offered by the systemic circulation that must be overcome to push blood through the circulatory system and create flow. Since BP can be related to the product of the cardiac output and the total peripheral resistance by applying Ohm's law in the hydraulic version, the variation of arterial blood pressure basically relies upon the changes of the total peripheral resistance. Most of the PPG morphology features extracted in this study are physiologically related to total peripheral resistance. Among them, PPGK and PIR_P ranked top 2 in the mean feature importance scores. Among the branch width based features, features extracted at the mid-level height (i.e., 50%, 66%, and 75%) of the PPG waveform ranked high in general. In addition, BW values generally showed high mean feature importance scores when compared to SBW, DBW, and BWR. Among the features extracted from the APG waveform, AI_b scored the seventh rank with a mean feature importance value of 0.43, but the remaining features scored very low ranks. For PCA features, PC2 showed the highest feature importance score with a mean value of 0.34. As a result, 28 features including the conventional PAT values and HR were finally determined as suitable BP estimation predictors.

2.4.2 Optimization of the BP Estimation Models

2.4.2.1 Frequency Component Separation

The performance of the BP linear models constructed by changing the cutoff frequency of the filter separating LFC/HFC of BP and features is shown in Table 2.5 and Figure 2.17. As shown in Table 2.5, modeling LFC and HFC of BP separately showed slightly better performance as compared to modeling without LFC/HFC separation. The optimal cutoff frequency was found to be 0.006 Hz.

Table 2.5 Performance of BP linear models with different cutoff frequencies of filter separating LFC/HFC across 413 validation recordings

Cutoff frequency	SBP			DBP		
	ME	SDE	MAD	ME	SDE	MAD
0[a]	<0.001	7.43	5.49	<0.001	4.17	3.00
0.001	-0.018	7.37	5.43	-0.004	4.14	2.98
0.002	-0.011	7.27	5.35	-0.005	4.10	2.95
0.004	-0.004	7.19	5.30	-0.002	4.08	2.93
0.006	**-0.002**	**7.17**	**5.29**	**-0.001**	**4.07**	**2.92**
0.008	-0.001	7.18	5.30	-0.001	4.07	2.93
0.016	-0.001	7.22	5.34	<0.001	4.09	2.95

[a]In the case of modeling without LFC/HFC separation.
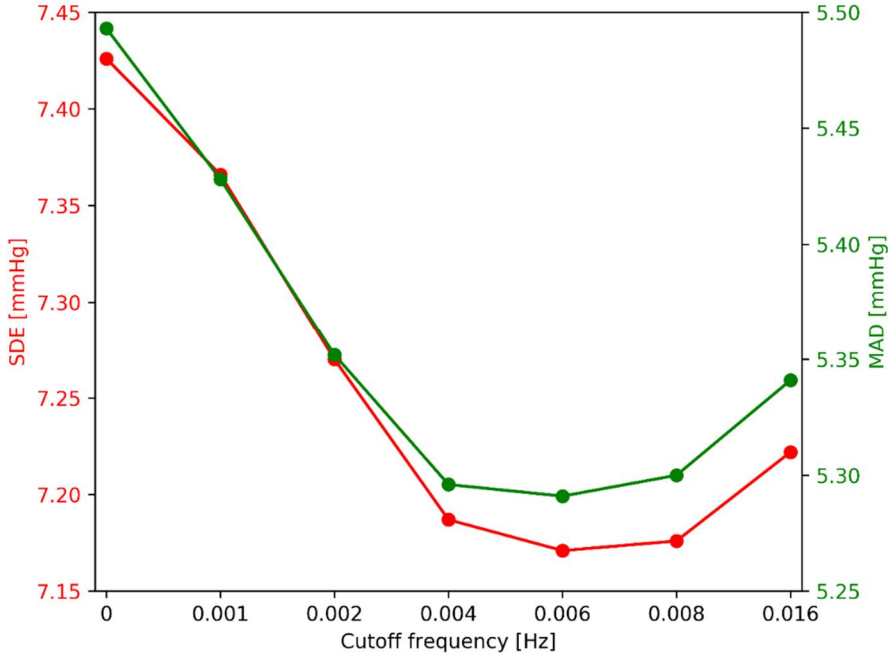
Figure 2.17 Overall SDE and MAD comparison between different cutoff frequencies. Red line corresponds to the SDE values and green line corresponds to the MAD values.

In order to prove the hypothesis that the relationship between BP and features can be clarified in a specific frequency band based on previous studies, frequency components of BP and features were separated. As a result of separately modeling LFC and HFC of BP with the optimal cutoff frequency at 0.006 Hz using linear regression, the performance of the estimation model was improved as compared to modeling both components of BP simultaneously. Similar results were found using non-linear regression methods such as ANN and RNN. The Pearson correlation coefficients and MI values between SBP and top 10 ranked features across 1376 subjects calculated for each of the LFC and HFC are shown in Table 2.6. The correlation values and mutual dependence

values of the features are generally lower in HFC, but almost all features are significantly better related to SBP in low frequency domain. Performing power spectral analysis, the power over low frequency bandwidth (0.0005–0.006 Hz) and the power over high frequency bandwidth (over 0.006 Hz) are calculated as the area under the power spectral density of SBP variation of each subject. As a result, the mean power across 1376 subjects is 101.16 $mmHg^2$ for LFC, and 4.96 $mmHg^2$ for HFC. Since the LFC of BP contains most of the components of BP variation, the enhanced relationships between BP and features in the LFC might improve the overall estimation performance.

Table 2.6 Pearson correlation coefficients and MI values between SBP and top 10 ranked features across 1376 recordings

Rank	Feature	LFC+HFC[a]		LFC[b]		HFC[c]	
		Pearson[d]	MI	Pearson[d]	MI	Pearson[d]	MI
1	PPGK	0.49	0.35	0.52	1.07	0.28	0.10
2	PIR_P	0.49	0.35	0.52	1.06	0.28	0.10
3	HR	0.34	0.37	0.33	1.06	0.32	0.12
4	PAT_{IT}	0.42	0.30	0.44	1.01	0.21	0.05
5	BW_{66}	0.42	0.35	0.45	1.09	0.18	0.08
6	BW_{75}	0.41	0.35	0.45	1.09	0.18	0.08
7	AI_b	0.29	0.24	0.31	0.99	0.12	0.05
8	PI_P	0.27	0.27	0.29	0.99	0.12	0.06
9	SBW_{66}	0.26	0.17	0.30	0.86	0.08	0.03
10	BWR_{50}	0.18	0.19	0.20	0.91	0.07	0.03

[a]Correlation between the raw SBP and the raw features.
[b]Correlation between the LFC of SBP and the LFC of features.
[c]Correlation between the HFC of SBP and the HFC of features.
[d]Absolute values of Pearson correlation coefficients.

2.4.2.2 Modelling Algorithms

The performance of the SBP models with different modelling algorithms is shown in Table 2.7. All modelling algorithms were constructed by separating LFC/HFC of BP and features with a cutoff frequency of 0.006 Hz. The performance measures were calculated for the LFC estimation model and the HFC estimation model separately. Since the ME values between different algorithms did not differ significantly, the performance comparisons between algorithms were conducted based on their SDE and MAD values. As shown in Table 2.7, ANN showed the best performance in LFC modelling, and RNN showed the best performance in HFC modelling. Similar results were found on the same analyses with DBP.

Table 2.7 Performance of SBP estimation models with different modelling algorithms across 413 validation recordings

Modelling algorithm	SBP					
	LFC			HFC		
	ME	SDE	MAD	ME	SDE	MAD
LR	-0.002	6.24	4.63	<0.001	2.20	1.42
RF	-0.135	6.32	4.59	0.003	2.15	1.37
ANN	**-0.025**	**6.07**	**4.48**	0.008	2.16	1.39
RNN	0.310	6.91	4.99	**0.077**	**2.14**	**1.36**

Several modelling algorithms including LR, RF, ANN, and RNN were evaluated. When comparing the estimation performances between these algorithms, the overall accuracy improved when using non-linear regression

methods as compared to LR in terms of SDE and MAD, potentially indicating nonlinear relationships between the features and BP values. However, due to the moderate degree of linear association between the features and BP values, the differences of the error values between LR and nonlinear modeling algorithms were minimal.

For LFC modelling, ANN showed the best performance in terms of SDE and MAD. Comparing the mean squared error values between models constructed by changing the number of hidden layers and the number of hidden nodes in the architecture of ANN, the optimal architecture was 100 hidden nodes with 1 hidden layer. In the case of the hidden layer activation function, models using tanh function outperformed models using relu or sigmoid functions.

In the case of RNN, it achieved the best performance in HFC modelling. However, it performed worse than ANN and LR in LFC modelling. There may be a few reasons for this lack of prediction performance, but one may be due to the problem of long-term dependencies [105]. Since LFC only contains slowly varying components below 0.006 Hz, the size of the time step of RNN modelling LFC should be large enough to properly capture the sequential change of features over time in the input data. A further study in which the period between each input time step may provide a suitable solution to this issue and such methods can be used to further improve estimation performance in the future.

Due to the range of complexities of the modelling algorithms used in this study, the duration for training varied widely. However, in terms of post optimization application of the algorithms, all of the methods were able to output a BP estimate within 600 microseconds using the current graphics processing unit (Geforce RTX 2080Ti; NVIDIA, Santa Clara, CA, USA), which is sufficient for pseudo real-time estimation of BP.

2.4.2.3 Comparison against Different Modelling Settings

The performances of the BP estimation models with varying settings are shown in Table 2.8. Comparing model 1 and model 2, it is confirmed that the estimation performance is improved by adding several PPG morphology features to the estimation parameters in addition to the conventional PAT values, making the model satisfy the AAMI standards. Moreover, it can be seen that the application of the LFC/HFC separation method (model 2 versus model 3) as well as using non-linear machine learning based regression method (model 3 versus model 4) further improve the estimation performance, then the model is rated grade A against the BHS standards.

Table 2.8 Performance of SBP estimation models with different modelling settings across 413 validation recordings

Model index	Modelling methods	SBP estimation							BP standards		
		ME	SDE	CP5	CP10	CP15	MAD	Corr[c]	AAMI	BHS	IEEE
1	LR (HFC+LFC)[a] – PAT[b]	<0.001	8.83	50	79	91	6.53	0.40	FAIL	B	C
2	LR (HFC+LFC)[a]	<0.001	7.43	57	85	94	5.49	0.58	PASS	B	B
3	LR(LFC) + LR(HFC)	-0.002	7.17	59	85	95	5.29	0.60	PASS	B	B
4	**ANN(LFC) + RNN(HFC)**	**0.052**	**6.92**	**62**	**87**	**96**	**5.07**	**0.63**	**PASS**	**A**	**B**

[a]In the case of modelling without LFC/HFC separation.
[b]In the case of modelling using only 4 PAT (PAT_V, PAT_P, PAT_{MD}, and PAT_{IT}) values as estimation predictors.
[c]Mean correlation value between the reference SBP and the estimated SBP across 413 validation recordings.

2.4.3 Performance of the Best-case BP Estimation Model

The best performing was model 4 in Table 2.8, which is obtained by modelling LFC of BP as ANN and HFC of BP as RNN using all 28 selected features as predictors. The detailed analysis of the best-case BP estimation model is shown in Table 2.9 and Figure 2.18. According to the estimated results, the model satisfies AAMI, BHS, and IEEE standards for both SBP and DBP estimates. In particular, in the case of SBP estimation, even though the high absolute magnitude of SBP led to large errors, the model was rated grade A against the BHS standards and nearly grade A against the IEEE standards (MAD of the model was 5.07 mmHg while grade A for the IEEE standards required MAD below 5 mmHg).
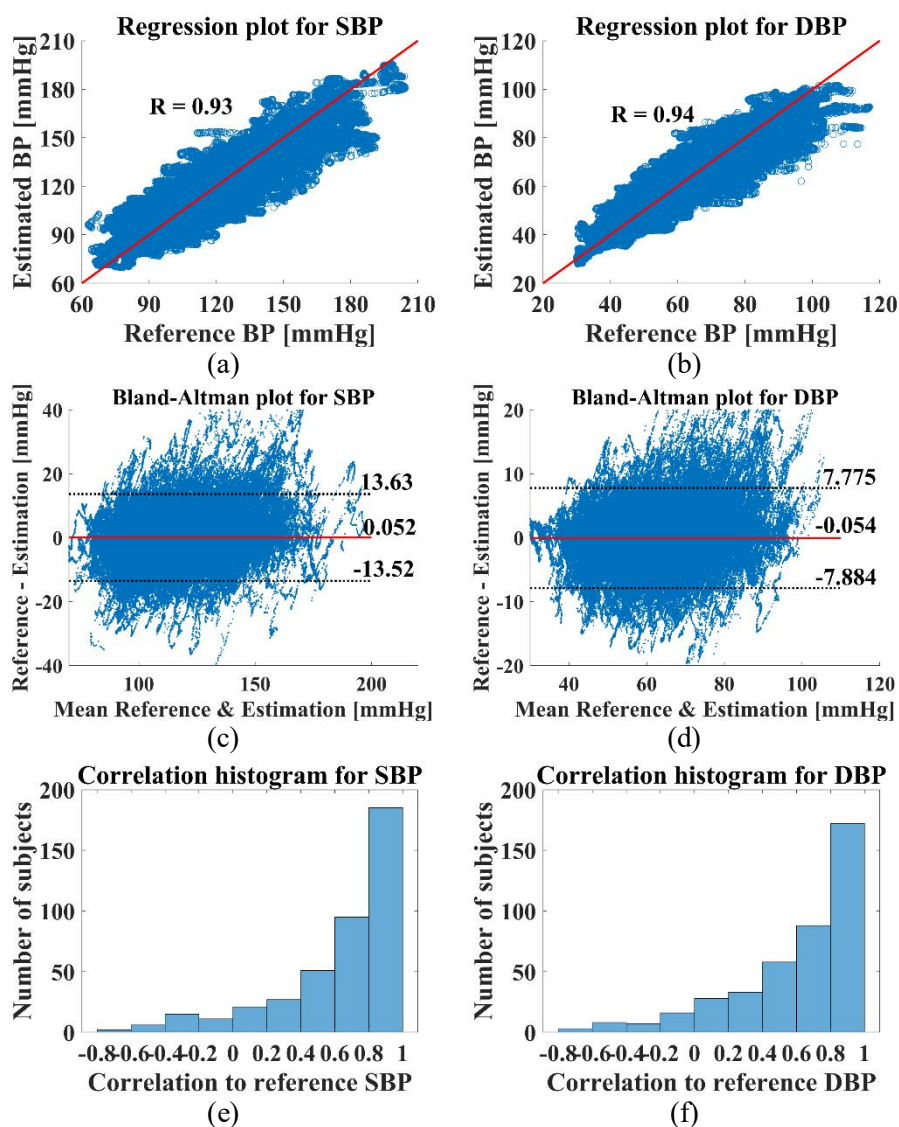
Figure 2.18 Performance of the best-case BP estimation model across 413 validation recordings. (a) Regression plot for SBP estimation; (b) Regression plot for DBP estimation; (c) Bland-Altman plot for SBP estimation; (d) Bland-Altman plot for DBP estimation; (e) Correlation histogram for SBP estimation; (f) Correlation histogram for DBP estimation.

Table 2.9 Performance of the best-case BP estimation model across 413 validation recordings

Performance Measure	SBP estimation model		DBP estimation model	
	Value	Evaluation	Value	Evaluation
ME (mmHg)	0.052	**PASS**[a]	-0.054	**PASS**[a]
SDE (mmHg)	6.92		3.99	
Cumulative Error < 5 mmHg (%)	62		84	
Cumulative Error < 10 mmHg (%)	87	**A**[b]	97	**A**[b]
Cumulative Error < 15 mmHg (%)	96		99	
MAD (mmHg)	5.07	**B**[c]	2.86	**A**[c]
Correlation to reference (mean $\pm$ STD)	0.63 $\pm$ 0.36		0.60 $\pm$ 0.36	

[a]Evaluation against the AAMI standards.
[b]Evaluation against the BHS BP monitor standards.
[c]Evaluation against the IEEE standards.

The distribution of the correlation values between the reference BP and the estimated BP across 413 validation datasets are shown in Figure 2.18(e) and Figure 2.18(f). For SBP, about 70 % of the subjects showed the correlation values higher than 0.6, and 45 % of the subjects showed higher than 0.8. Similar trends were seen on the same analyses with DBP. Unlike most of the previous studies used only error-based validation criteria, these results present the degree of association in trends between the reference BP and the estimated values. However, as some cases still show low or opposite correlation, a further study is warranted to further improve the estimation performance in terms of correlation.

The performances of the BP estimation models with respect to BP ranges across 413 validation recordings are shown in Table 2.10. The model satisfies three international BP standards within BP ranges between 70 mmHg and 170

mmHg for SBP and BP ranges between 30 mmHg and 100 mmHg for DBP. Although the model failed to track the reference BP with a clinically applicable accuracy beyond the specified BP ranges, the measurable BP ranges of the model are wide enough to classify all BP categories including "stage 2 hypertension" which is defined as an average SBP of at least 140 mmHg or an average DBP of at least 90 mmHg [106].

Table 2.10 Performance of the best-case BP estimation model with respect to BP ranges across 413 validation recordings

BP range (mmHg)	Observations (%)	Performance measures							BP standards		
		ME	SDE	CP5	CP10	CP15	MAD	Corr[a]	AAMI	BHS	IEEE
SBP estimation model											
<70	0.1	-8.77	7.75	40	74	88	8.77	-0.32	**FAIL**	**C**	**D**
70-90	6.6	-4.93	6.80	57	80	90	6.14	0.37	**PASS**	**B**	**C**
90-110	34.9	-1.72	5.93	66	89	97	4.58	0.60	**PASS**	**A**	**A**
110-130	35.9	0.59	6.16	63	90	97	4.67	0.64	**PASS**	**A**	**A**
130-150	16.6	2.42	6.81	56	86	96	5.46	0.59	**PASS**	**B**	**B**
150-170	5.1	4.82	7.89	51	76	89	6.71	0.52	**PASS**	**B**	**C**
>=170	0.8	11.11	13.88	26	46	62	14.09	0.29	**FAIL**	**FAIL**	**D**
DBP estimation model											
30-40	2.1	-2.05	3.57	79	96	100	2.93	0.71	**PASS**	**A**	**A**
40-50	14.1	-1.63	3.48	85	97	100	2.73	0.52	**PASS**	**A**	**A**
50-60	29.4	-0.70	3.42	87	98	100	2.55	0.61	**PASS**	**A**	**A**
60-70	31.4	-0.12	3.56	86	98	100	2.63	0.59	**PASS**	**A**	**A**
70-80	15.9	1.28	3.92	81	97	100	3.07	0.50	**PASS**	**A**	**A**
80-90	5.6	2.48	4.82	72	92	98	3.98	0.43	**PASS**	**A**	**A**
90-100	1.4	5.03	6.10	56	79	92	5.85	0.35	**PASS**	**B**	**B**
100-110	0.2	12.63	5.64	10	30	67	12.63	0.29	**FAIL**	**FAIL**	**D**

[a]Mean correlation value between the reference BP and the estimated BP across 413 validation recordings.

For the purpose of external validation, the constructed BP estimation model was evaluated using an external dataset from the MIMIC III waveform database [107]. Data from part 0 of the MIMIC III waveform database matched subset was used. Data loading, pre-processing and feature extraction processes were performed in the same manner as described above. As a result, a total of 750,898 pairs of BP and features from 334 subjects are extracted. The estimation performance of the model across the external validation dataset is shown in Table 2.11. As shown in Table 2.11, the model satisfies AAMI, BHS, and IEEE standards for both SBP and DBP estimated in the external database, indicating that the developed BP estimation model can be applied to data with different measurement modalities and different demographics.

Table 2.11 Performance of the best-case BP estimation model across 334 external validation recordings

Performance Measure	SBP estimation model		DBP estimation model	
	Value	Evaluation	Value	Evaluation
ME (mmHg)	-0.006	**PASS**[a]	-0.004	**PASS**[a]
SDE (mmHg)	7.04		4.77	
Cumulative Error < 5 mmHg (%)	61		86	
Cumulative Error < 10 mmHg (%)	87	**A**[b]	96	**A**[b]
Cumulative Error < 15 mmHg (%)	95		98	
MAD (mmHg)	5.13	**B**[c]	2.81	**A**[c]
Correlation to reference (mean $\pm$ STD)	0.52 $\pm$ 0.40		0.53 $\pm$ 0.38	

[a]Evaluation against the AAMI standards.
[b]Evaluation against the BHS BP monitor standards.
[c]Evaluation against the IEEE standards.

Example plots of the reference BP and the BP estimates from four representative subjects in the external database are shown in Figure 2.19.
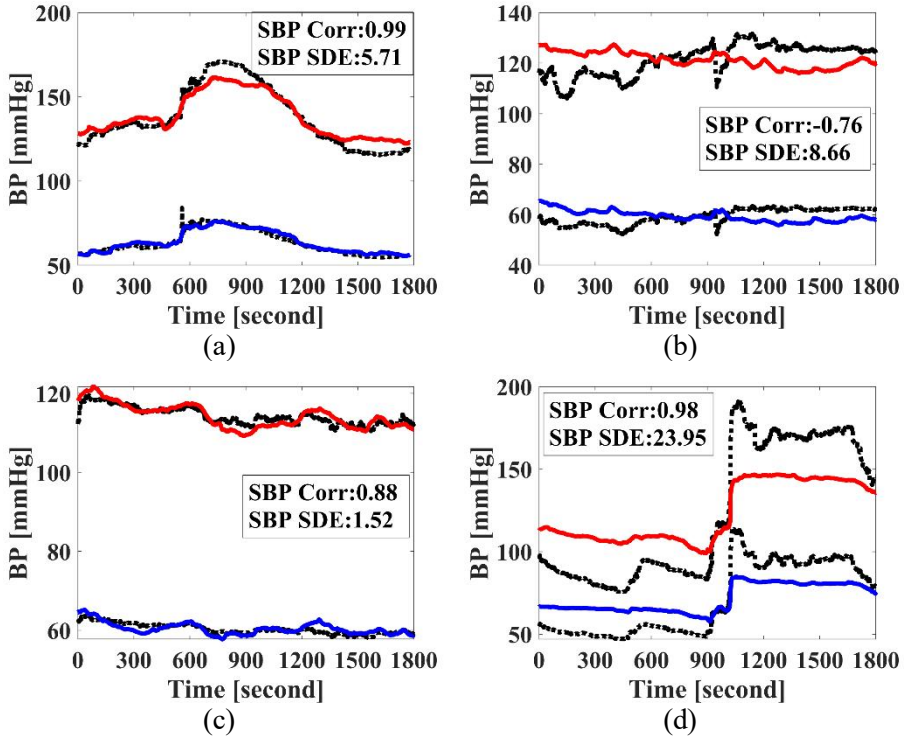
Figure 2.19 Example plots of estimated BP and reference BP in 4 representative external validation recordings. Solid red line corresponds to the estimated SBP, solid blue line corresponds to the estimated DBP, and dotted black line corresponds to the reference BP. (a) The recording with the highest SBP correlation; (b) The recording with the lowest SBP correlation; (c) The recording with the lowest SBP SDE; (d) The recording with the highest SBP SDE.

As shown in Table 2.11 and Figure 2.19(b), in terms of correlation to reference BP, the performance was degraded, which might be caused due to the lower BP variations in the test dataset (the standard deviation values of SBP were 10.3 mmHg for validation dataset and 8.6 mmHg for test dataset), or incorrect PAT values due to the inter-waveform alignment issue. As shown in

Figure 2.19(d), a sample with very low or very high BP values tended not to be accurately estimated. It might be caused due to the limited number of subjects with very high or very low BP values in the training dataset, or it may have been caused by sharp changes in BP during this particular surgery, which is not usually observed. However, the overall trend of BP variations was well tracked as indicated by the high correlation value in Figure 2.19(d).

2.4.4 Limitations

There are a few limitations to mention. First, there is a possibility of consistent delay between the signals due to the experimental setup. The exact data collection logic is not known, but the average PAT_{IT} was around 650 ms, which is extremely large compared to previous reports of PAT from ECG to finger PPG. Although PAT varies largely based on the point on PPG at which PAT is extracted, this seems to be quite large compared to PAT_{ABP} which averages around 150 ms. Comparing these values to previous studies with similar setups, it is likely that there exists a delay between ECG, ABP, and PPG. However, this delay was consistent in the entire dataset with all subject with PAT_{IT} ranging between 600 ms to 670 ms with mean across all subjects at 659 ms and standard deviation at 30 ms, which shows a general shift of the PAT value from the expected range around 300 ms. We have verified with the creators of the database the consistency of this delay throughout all recordings

used. Through the calibration procedure, it is ensured that this delay does not affect the analyses of this study.

The second limitation of this study was the variation in the surgery types used in this study. Although the wide range of surgeries may represent wide sources of hemodynamic change, it also represents a source of inconsistency in analyses. Different types of surgeries with different anesthesia calls for an in-depth analysis based on anesthesia use and subsequent BP change, but this could not be done as the timing for the dosing was not exact according to the authors of the database. Furthermore, certain recordings may include hemorrhage and subsequent blood transfusion events which would distort pulse wave transmission, making the data unacceptable for some of the analyses above. However, by pre-processing the dataset with visual inspection, we believe we have eliminated much of recordings or parts of recordings with low SNR, and we have performed the analyses above without taking the type of surgery into consideration as any dataset with such a large subject pool would have sources of variations that cannot be accounted for.

Another limitation is that the VitalDB database used in this study only contains biosignals obtained from patients undergoing surgery. Most of the data was measured from motionless subjects who were in supine position. However, previous research has shown that postural changes affect the morphology of PPG [108]. In terms of ubiquitous NCBPM, the underlying mechanism of BP variation during surgery may be different as compared to the ones dominating

the circadian fluctuations of BP. There are several physiological mechanisms that regulate BP. Short-term regulation of BP is controlled by the autonomic nervous system, which is known as baroreceptor reflex, and long-term regulation of BP is controlled by the renin-angiotensin-aldosterone system (RAAS) or by release of Anti Diuretic Hormone (ADH). Since most BP variations during surgery are caused by sympathetic response triggered from the autonomic nervous system, the BP estimation model developed in this study using surgical biosignal database might not be applicable to long-term BP perturbation mechanisms. Therefore, a further study is warranted to validate the estimation model against data measured in less controlled environment, which will be conducted in chapter 3.

2.5 Conclusion

In general, previous studies of BP estimation have analyzed different features and have used small homogeneous subject pools to generate models of BP. However, these BP estimation models are not extendable for general use due to the nature of these experiments and are not properly validated for clinical use. This is the first study to use a large heterogeneous dataset to validate the potential of PAT, PTT, and diverse PPG morphology features as predictors of BP comprehensively, and to develop the clinically usable BP estimation models using these predictors. The key findings of the study were that 1) PAT outperform PTT as an indicator for BP, 2) 28 features including several PPG morphology features and PAT were determined as suitable BP predictors, in particular two PPG morphology features (PPGK and PIR_P) outperformed PAT, and 3) BP estimation models constructed by modelling LFC using ANN and HFC using RNN with selected 28 predictors showed the best estimation performance, satisfying the three relevant international standards for BP monitors in validation and in external validation datasets.

* Large sections of this chapter were published previously in *IEEE Journal of Biomedical and Health Informatics* (Seungman Yang, et al. "Estimation and Validation of Arterial Blood Pressure using Photoplethysmogram Morphology Features in conjunction with Pulse Arrival Time in Large Open Databases".

IEEE Journal of Biomedical and Health Informatics, 2020) [109], and in *Journal of clinical medicine* (Joonnyong Lee, Seungman Yang, et al. "Analysis of Pulse Arrival Time as an Indicator of Blood Pressure in a Large Surgical Biosignal Database; Recommendations for Developing Ubiquitous Blood Pressure Monitoring Methods". *Journal of clinical medicine*, 2019) [104].

Chapter 3

Development of the Single Chest-worn Device for Non-invasive Continuous Arterial Blood Pressure Monitoring

3.1 Introduction

Although numerous indirect approaches for BP estimation have been developed over the recent decades, almost all researchers have been focusing on PTT based methods. In order to measure PTT, which is defined as the time delay for the arterial pulse to propagate between two arterial sites, both proximal and distal time references should be detected. Multiple methods to measure proximal and distal time references have been proposed so far. Most widely accepted method to measure PTT is to detect R-peak as proximal time reference by measuring ECG on the chest and to detect a point on distal pulse waveform by measuring PPG, which is known as PAT. Some studies have used impedance cardiogram (ICG), a measure of changes in thoracic electrical impedance, to detect a proximal time reference [75, 110]. Since ICG has a characteristic point called B point, which coincides with the moment when the aortic valve opens, it can be used to measure a proximal waveform for estimation of PTT through central arteries. In recent, due to the advances in sensor technology and digital signal processing, ballistocardiogram (BCG) or seismocardiogram (SCG), which can be measured by attaching an accelerometer on body, have been widely analyzed to detect a proximal waveform [22, 26, 41, 42]. Multi-site channels of PPG system attached to diverse body points such as finger, toe and earlobe have been also widely developed for PTT measurement [111]. In addition, PTT measurement methods

using various biosignals such as echocardiogram, phonocardiogram, and tonometry have been proposed. However, almost all of the proposed methods commonly require two or more modules with bulky electrodes to measure the arterial pulse waves from two arterial sites. Most studies have mainly focused on generating and validating BP estimation models, and little consideration has been given to the practicality and user compliance of the BP monitoring system.

In order to overcome this issue to facilitate ubiquitous BP monitoring, we developed a wearable and unobtrusive wireless single chest-worn device, which can provide users with utmost convenience in continuous BP monitoring. The device simultaneously measures ECG and PPG to extract BP estimation predictors, and additionally measures body movement and SCG through an accelerometer from the torso. The general concept of the developed device is shown in Figure 3.1.
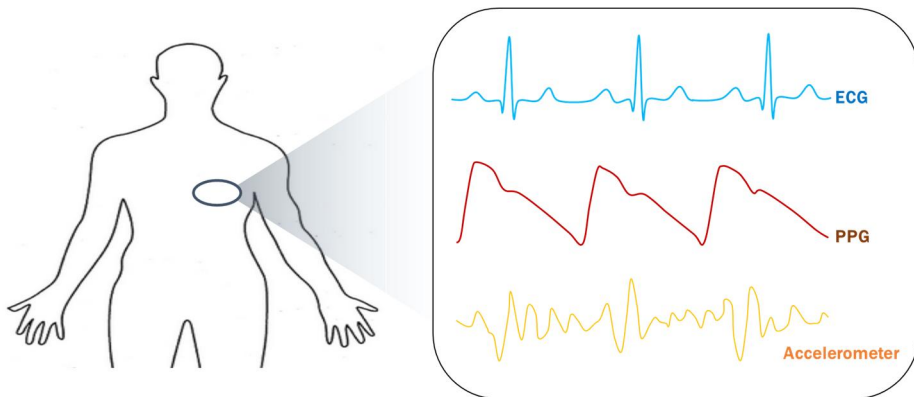
Figure 3.1 The concept of the proposed BP monitoring system.

Our preliminary study using the developed device showed seemingly decent BP estimation performance against 20 healthy males with a multivariate model using the SCG amplitude in conjunction with PTT, trained in the dataset from 10 subjects [112]. However, the developed BP estimation model is not properly evaluated for clinical use since the small homogeneous subject pools are used to train and validate the model. In this study, we tested the BP estimation model constructed in chapter 2 on the dataset measured by the developed device to verify the model's applicability to data with single wearable measurement modality.

3.2 Development of the Single Chest-worn Device

3.2.1 Hardware Development

A patch-type hardware was developed to measure ECG and PPG simultaneously in a single module for extracting PAT and PPG morphology features as BP indicators. In addition, an accelerometer was used to detect the body movement and measure SCG for an auxiliary purpose. The overall system block diagram is shown in Figure 3.2.

Since the blood perfusion encountered at the chest beneath the skin was not abundant for PPG measurement compared to other peripheral body parts such as the finger, toe, and earlobe, three independent PPG channels were used to improve the SNR of the chest PPG. Each PPG channel consists of one green photo-emitter LED (XZM2DG55W-3, SunLED, USA) and two silicon photodiodes (VBPW34S, Vishay, USA). The green LED has a peak wavelength of 520 nm, and driven by a peak current of 30 mA. The distance between the center of the photodiode and the LED is set to 4 mm. In order to provide spatial diversity to reduce the dependence of estimations with respect to the sensor's placement, the three PPG channels were placed apart by 25 mm from each other. Each output current from the three optical sensor pairs is converted to voltage using a trans-impedance amplifier (TIA).

In addition to using a multi-dimensional PPG channels, ambient light cancellation and offset DC feedback techniques are implemented in order to increase the SNR of the chest PPG. Ambient light cancellation incorporates a proprietary scheme to cancel the photodiode current generated by ambient light up to 200 μA, allowing the sensors to work in high ambient light conditions. In order to accentuate the waveform features, the pulsatile component of the PPG waveform, which is usually called the alternative current (AC) component, should be amplified. The fundamental solution to amplify the AC component of the PPG waveform is to increase the intensity of light illuminating the chest region. However, using high intensity of light may cause the TIA circuit to be saturated since it also amplifies the direct current (DC) component of the PPG waveform that relates to the tissues and to the average blood volume. Therefore, we implemented offset DC feedback technique to regulate the DC level of PPG for preventing the circuit from the saturation while amplifying AC level for enhancing the SNR of the chest PPG. The voltage level of the TIA circuit is monitored periodically, and when this value exceeds a preset threshold, the amount of the feedback current injected to the TIA circuit is controlled via the digital to analog converter (DAC) to regulate the DC level of PPG.

For ECG measurement, two-electrode configuration was employed with common-mode biased voltage to form a single lead of ECG across the chest. Two electrodes were placed apart by 5 cm from each other to minimize the size

of the device while ensuring sufficient signal strength. The surface of bipolar electrode pair is coated with platinum to increase bio-compatibility.

For the auxiliary purpose, an analog accelerometer (ADXL327, Analog Devices, USA) was used to detect body movement and to measure SCG.

All biosignals were digitized using a high resolution (24-bit) analog-to-digital converter (ADC) (ADS1298, TI, USA) at 100 Hz.

On power control unit, power hold circuit for toggling the device ON and OFF with a momentary button press (more than 3 seconds) that controlled a latching transistor power switch was implemented. Furthermore, for minimizing LED power consumption, the LED pulse width and the LED settling time were programmed to control the dimming frequency and timing of the LEDs illuminating. The overall system power was supplied by a 280 mAh lithium polymer battery (MP452530, Maxpower, China), which is rechargeable via battery charge circuit with a micro-USB cable.

All the above mentioned biosignal processing units and power control unit were programmed via a micro control unit (MCU) (ATmega168, Microchip Technology, USA). The processed biosignal data were then transmitted to an external data acquisition software via a Bluetooth Low Energy (BLE) module (BoT-CLE310, Chipsen, South Korea).
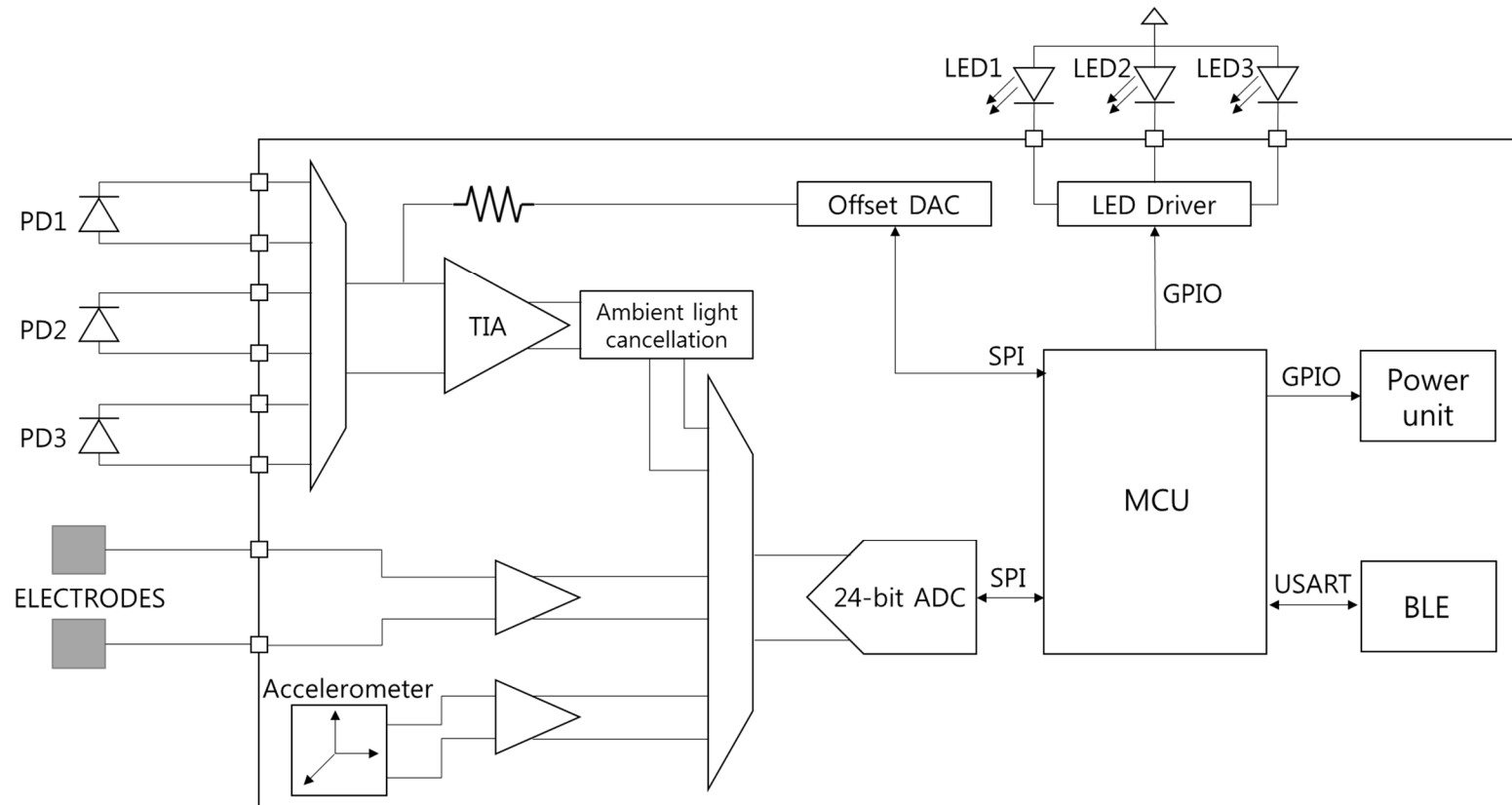
Figure 3.2 System block diagram.

The design of a printed circuit board (PCB) and a case was implemented through the hardware evolution process as shown in Figure 3.3. The first version of the device was developed using a rigid PCB design. However, given that the device must be attached to the chest, PCB and case of the device should be able to bend to conform to the curvature of the chest. From this point of view, the design of the PCB has gradually upgraded from version 1 to version 4. In version 2, the entire circuit system was divided into three parts, each composed of rigid PCB islands, and these are connected with connectors to provide flexibility into the device. However, the connectors with bulky wires limited the minimization of the device. In version 3, the device was developed by configuring the entire system with a flexible PCB design, but the circuit systems on the flexible PCB caused unstable signal integrity and deteriorated the system performance. Finally, in version 4, we developed the device with rigid-flex PCB which was composed of three rigid pieces connected by flexible connecting parts to conform the device to the curvature of the chest with electrically stable configures. Then, a hard case with curved design for torso curvature was developed at version 5 as shown in Figure 3.3.
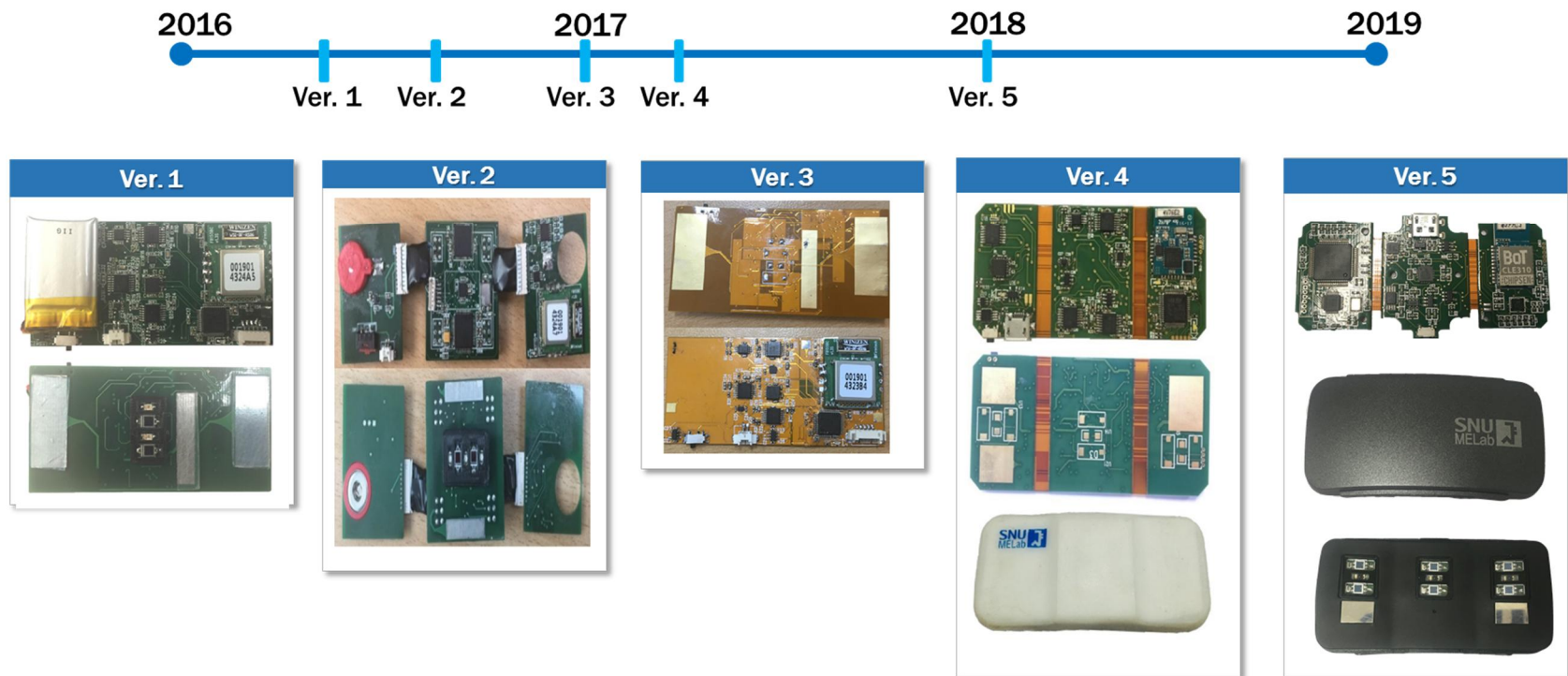
Figure 3.3 Hardware evolution.

3.2.2 Software Development

In this study, two types of data acquisition platforms were used for obtaining biosignal data from the developed device with the reference BP as shown in Figure 3.4.

First, for the purpose of monitoring quality of the biosignals and saving the data in the in-lab condition, a graphical user interface (GUI) data acquisition software was developed using MATLAB. This collects biosignal data from the developed device and reference BP data from the finger-cuff type BP measurement device (Finometer, Finapres Medical Systems, Netherlands) based on the volume clamp method via a serial port, and displays the raw waveforms of biosignals including ECG and PPG and the pre-processed segments for monitoring signal quality. The signals and reference BP are recorded by pushing the saving button, and the recording time is shown on the panel. Event markers can be added during recording.

Second, in order to obtain the developed device data with time-synchronized data from multiple commercial patient monitor devices including arterial blood pressure from the patients undergoing anesthesia surgery, we integrated the developed device data acquisition protocol into the Vital Recorder program developed by the Seoul National University Hospital Department of Anesthesia [78]. The Vital Recorder program is a free research tool for recording of time-synchronized physiological data from multiple intraoperative devices and patient monitors.
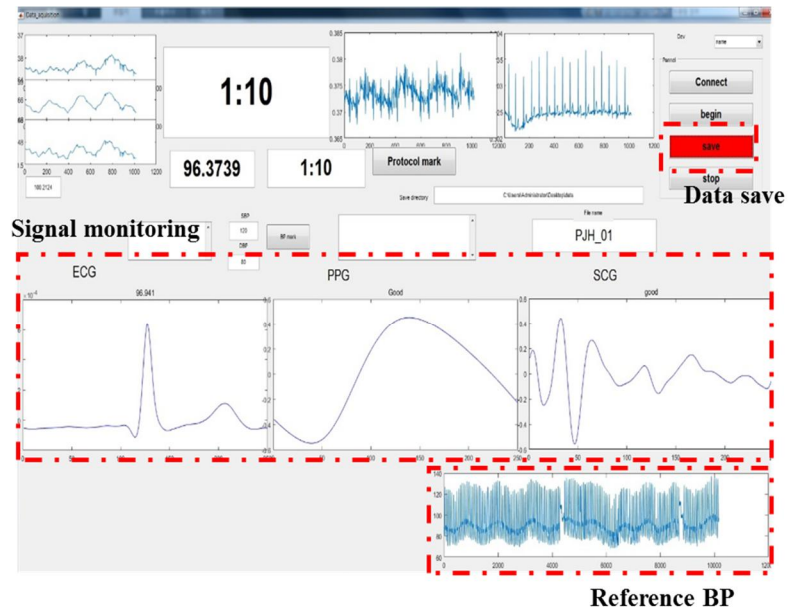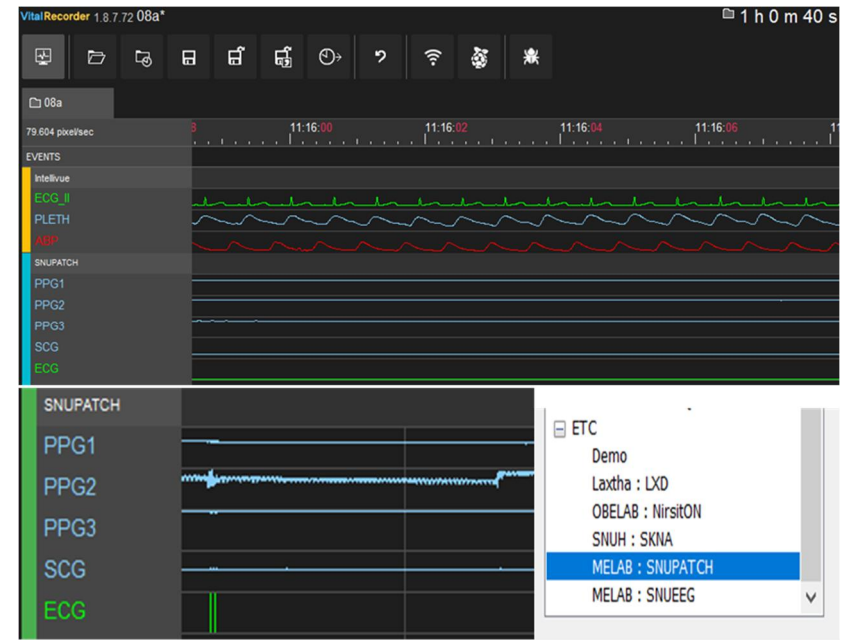
Figure 3.4 Data acquisition platform. (a) A graphical user interface data acquisition platform for the in-lab condition; (b) The Vital Recorder program for the anesthesia surgery condition.

3.2.3 Clinical Trial

Thirty-one healthy males $(39 \pm 12$ years old) without any history of cardiovascular conditions were recruited for data acquisition. The demographic and BP characteristics of the subjects are shown in Table 3.1.

Table 3.1 Demographic and BP characteristics of the data (N=31)

Characteristics	Subjects
Age (years)	39 ± 12 (range 21–64)
Height (cm)	171 ± 6
Weight (kg)	70 ± 8
BMI (kg/m^2) [a]	24 ± 3
Rest SBP (mmHg)	124 ± 11
Rest DBP (mmHg)	79 ± 9

[a]Body mass index.

The study was approved by the Institutional Review Board of Seoul National University Hospital (H1701-111-826). Written informed consent was obtained from all subjects. The developed device was placed over the skin of the sixth left costal cartilage. Finometer continuous BP monitor was used as a reference. The cuff from the reference device was worn around the right index finger. We acquired the biosignal data from the device and the reference BP while inducing hemodynamic changes in three ways. The three types of intervention employed were mental stress, cold pressor test, and cycling exercise. The experimental procedure for each intervention is shown in Figure 3.5.

• Mental stress

Rest 5-min	Mental stress 5-min	Recovery 5-min

• Cold pressor test

Rest 5-min	Feet immersion 3~5-min	Recovery 5-min

• Cycling exercise

Rest 5-min	Cycling 10-min	Recovery 5-min
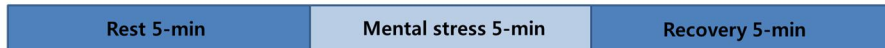
Figure 3.5 The experimental procedures of three BP interventions.

Mental stress protocol induces hemodynamic changes by giving a subject a task that causes various mental stresses such as mental arithmetic test and the Stroop test. According to the previous studies, mental stresses increase secretion of cortisol and adrenocorticotropic hormone (ACTH) and raise BP [113]. In this study, mental arithmetic test and the Stroop color-word test were performed. For the mental arithmetic test, the subject calculated four-digit numbers displayed on the screen into one-digit numbers, and decided that the final result was even or odd by pushing the designated buttons on the screen. For the Stroop color-word test, the subject read the colors of the words displayed on the screen, and decided if the word meaning and font color are congruent or not by pushing the designated buttons on the screen. The protocol was performed for 5 minutes while giving a time of 5 seconds per question. The subjects were told that they could earn a monetary bonus for speed and accuracy on the task.

Cold pressor test triggers in subjects a vascular sympathetic activation, an increase in total peripheral resistance and an increase in BP [114]. In this study, the subject immersed her/his feet into a 5-10 ℃ water bath for a period of 3-5 minutes to obtain a cold pressor recording.

Cycling exercise is one of the most widely used interventions to induce hemodynamic changes, especially since it can greatly increase BP quickly [21, 76]. In this study, the subject cycled with her/his torso in an upright position and was required to keep their upper body still during exercise. During cycling, the same intensity of the exercise was applied to all subjects.

5 minutes of rest and 5 minutes of a recovery period prior to and after each BP intervention were given. During the whole procedures, subjects were studied in sitting position in a quiet room. The data from two subjects were not used in any analyses due to their poor chest plethysmography signals. Four other subjects were excluded from the analyses because the reference BP values were not properly recorded due to the data acquisition software mal-function. Finally, 39,832 data pairs of BP and features from 25 subjects were extracted.

3.3 Development of the Transfer Function

3.3.1 Finger PPG versus Chest PPG

In chapter 2, the BP estimation model was constructed using ECG and PPG measured from the VitalDB database. In this database, PPG waveform was measured from the finger. However, PPG waveform was measured from the finger in the developed single chest-worn device dataset. When comparing the typical PPG waveform morphology at the chest derived from the single chest-worn device dataset to the typical PPG waveform morphology at the finger derived from the VitalDB database, there were significant differences in the characteristics of morphologies between finger PPG waveform and chest PPG waveform. As shown in Figure 3.6, when a triangle is formed by connecting two adjacent valley points and peak point of the PPG waveform, the typical finger PPG waveform was formed narrower than the triangle. On the contrary, the typical chest PPG waveform was formed wider than the triangle.

(a)   (b)
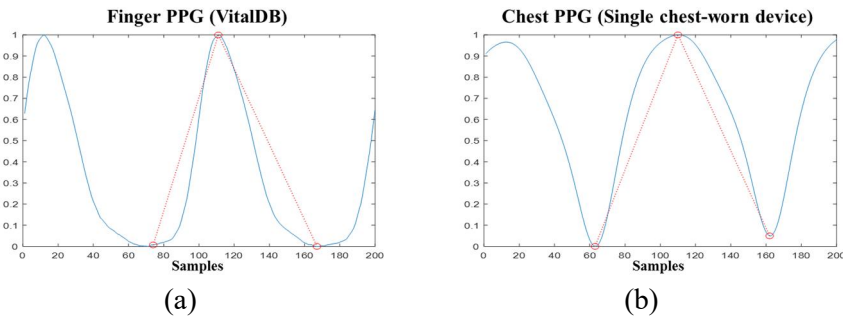
Figure 3.6 Typical morphologies of finger PPG waveform and chest PPG waveform. (a) The typical morphology of finger PPG waveform derived from

the VitalDB database; (b) The typical morphology of chest PPG waveform derived from the single chest-worn device dataset.

This difference in characteristics also affects the extracted PPG morphology features. As a result of two-sample t-test, there were significant differences in all of the PPG morphology features between finger PPG and chest PPG. The box plots of the top 3 important PPG morphology features (PPGK, PIR_P, and BW_{66}) derived from the finger and the chest are shown in Figure 3.7.

(a)　　　　　　　(b)　　　　　　　(c)
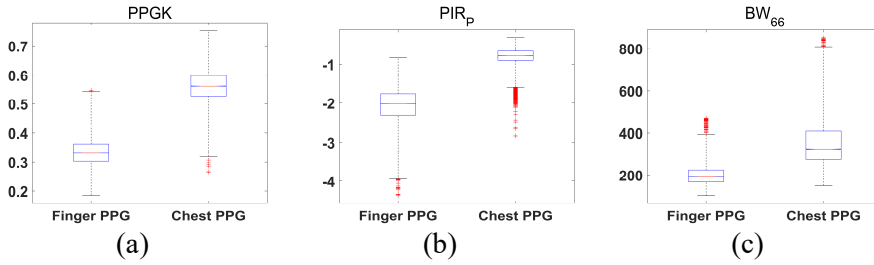
Figure 3.7 Box plots of the top 3 important PPG morphology features derived from the finger and the chest. On each box, the central mark indicates the median, and the bottom and top edges of the box indicate the 25th and 75th percentiles, respectively. The whiskers extend to the most extreme data points not considered outliers, and the outliers are labeled with the '+' symbol. (a) Box plot for PPGK; (b) Box plot for PIR_P; (c) Box plot for BW_{66}.

When blood is ejected from the heart, the pulse wave begins to travel forward along the blood vessels. When the pulse wave reaches the end of the blood vessel at the peripheral artery, a part of the wave is reflected and travels in the backward direction. As a result, the PPG waveform morphology at a

given arterial site is determined as the sum of the forward and backward wave components at that site. Since there is no time delay between the forward and backward waves at the end of the blood vessel, the PPG waveform tends to become narrower and sharper as the distance from the heart increases. From this point of view, it can be deduced that the arterial sites at the chest are much closer to the heart than those at the finger.

3.3.2 The Concept of the Transfer Function

Due to the significant differences in the characteristics of morphologies between finger PPG waveform and chest PPG waveform, PPG morphology features extracted from the chest need to be translated to the corresponding finger PPG morphology features prior to inputting them to the BP estimation model constructed in chapter 2. Therefore, the objective of this study is to develop a transfer function model mapping the chest PPG morphology features to the corresponding finger PPG morphology features in order to apply the clinically usable BP estimation model derived from large heterogeneous subject pool to the single chest-worn device. The overall concept of the transfer function is shown in Figure 3.8.
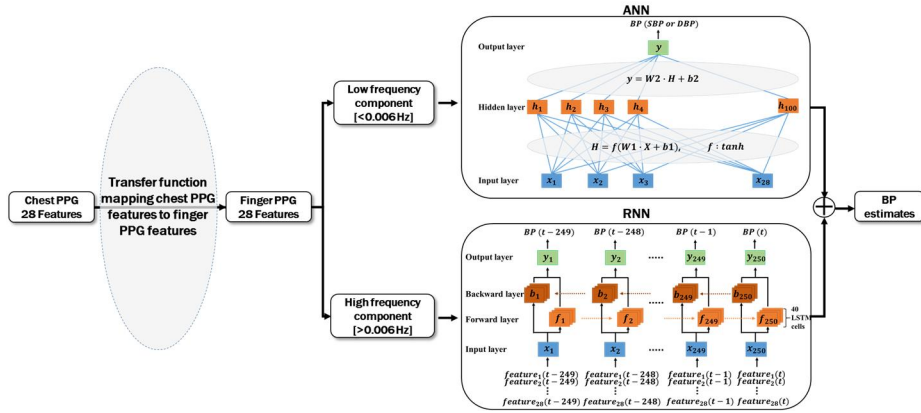
Figure 3.8 The concept of the transfer function model.

3.3.3 Data Acquisition for Modelling of the Transfer Function

For the development of the transfer function, a dataset including the finger PPG waveform and the chest PPG waveform measured simultaneously should be acquired. In this study, two datasets with different experiment settings were obtained.

For the first dataset, nine pediatric patients aged between 3 years and 12 years who were scheduled for ophthalmic surgery or neurosurgery were enrolled. This study was approved by the Institutional Review Board of Seoul National University Hospital (H1907-088-1049). Written informed consent was obtained from all parents. During the surgery, ECG and finger PPG signal were acquired with the commercial patient monitor (IntelliVue MX800, Philips Healthcare, Netherlands) and chest PPG signal was acquired with the single

chest-worn device. All signals were recorded at sampling frequency of 100 Hz by the Vital Recorder program.

Similar dataset was obtained from five healthy males aged between 27 years and 30 years in the in-lab condition. This study was approved by the Institutional Review Board of Seoul National University Hospital (H2012-047-1180). ECG and finger PPG signal were acquired with the commercial patient monitor (SOLAR8000M, GE Healthcare, England) and chest PPG signal was measured by the single chest-worn device simultaneously in each experiment. All biosignals of each subject were recorded for 10 minutes at the rest status in supine position.

Totally, chest and finger PPG matching dataset from 14 subjects were obtained to develop the transfer function.

3.4 Results and Discussion

3.4.1 Construction of the Transfer Function

The entire dataset consisting of 14 subjects was randomly divided into two sets; 16,143 chest/finger matching PPG morphology features from 10 subjects were used to train the transfer function model and 4,543 chest/finger matching PPG morphology features from 4 subjects were used for validation. Since there were no significant differences in four PAT values (PAT_V, PAT_P, PAT_{MD}, and PAT_{IT}) and HR between finger PPG and chest PPG, only 23 PPG morphology features were used.

Before inputting the chest PPG morphology features to the transfer function model, 23 chest PPG morphology features were standardized using the whole chest PPG dataset from 14 subjects for data scaling. Then, the transfer function model output for each subject was de-standardized using the whole finger PPG dataset from 14 subjects.

The modelling algorithm for the transfer function used in this study was ANN. The architecture of the transfer function model is shown in Figure 3.9. Parameters of ANN were chosen after considering multiple different combinations. The transfer function model in this study consisted of an input layer, two hidden layers with 100 nodes and 40 nodes using sigmoid function as the activation functions respectively, and 23 nodes for finger PPG morphology features prediction in the output layer. MSE was used as the cost

function. To optimize the network, an ADAM optimizer with initial learning rate of 0.001 was used. The training of the transfer function was done using Python and Tensorflow.
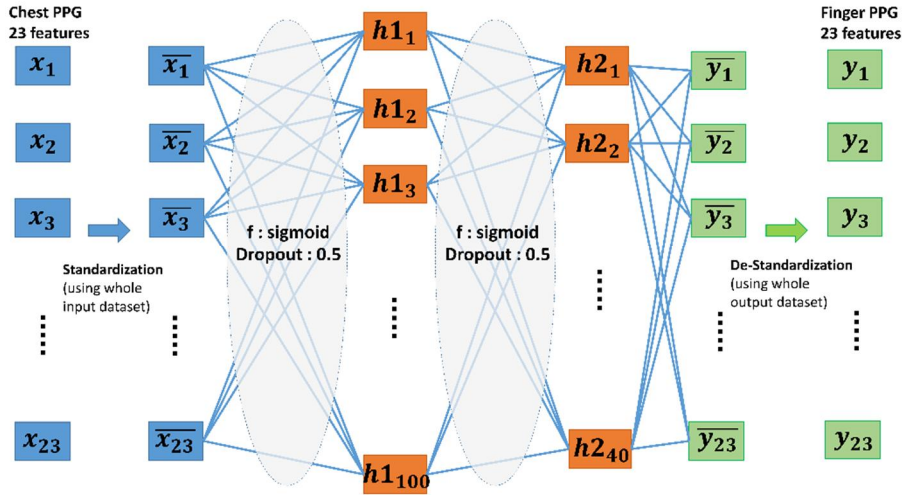
Figure 3.9 The architecture of the transfer function model.

3.4.2 Test of the BP Estimation Model

The performance of the BP estimation model across the single chest-worn device dataset from 25 subjects without applying the transfer function model is shown in Table 3.2 and Figure 3.10. As shown in Table 3.2, although DBP estimation model showed seemingly decent performance with satisfying all of the international BP standards, SBP could not be predicted to a satisfactory level due to higher errors. The SBP estimation model does not satisfy the AAMI standards and BHS standards, and is rated grade D against the IEEE standards.

Figure 3.10 Performance of the BP estimation model across the single chest-worn device dataset without applying the transfer function. (a) Regression plot for SBP estimation; (b) Regression plot for DBP estimation; (c) Bland-Altman plot for SBP estimation; (d) Bland-Altman plot for DBP estimation.

Table 3.2 Performance of the BP estimation model across the single chest-worn device dataset without applying the transfer function

Performance Measure	SBP estimation model		DBP estimation model	
	Value	Evaluation	Value	Evaluation
ME (mmHg)	-0.015	**FAIL[a]**	-0.014	**PASS[a]**
SDE (mmHg)	13.18		6.42	
Cumulative Error < 5 mmHg (%)	33		59	
Cumulative Error < 10 mmHg (%)	59	**FAIL[b]**	89	**B[b]**
Cumulative Error < 15 mmHg (%)	78		97	
MAD (mmHg)	10.07	**D[c]**	4.96	**A[c]**
Correlation to reference (mean $\pm$ STD)	0.43 $\pm$ 0.45		0.25 $\pm$ 0.52	

[a]Evaluation against the AAMI standards.
[b]Evaluation against the BHS BP monitor standards.
[c]Evaluation against the IEEE standards.

Significant differences in the characteristics of morphologies between the finger PPG waveform and the chest PPG waveform might cause poor BP estimation performance. The performance of the BP estimation with applying transfer function model in the single chest-worn device dataset are seen in Table 3.3 and Figure 3.11. As shown in Table 3.3, there are significant improvements in all of the performance measures. With the transfer function model, SBP estimation satisfies the BHS standards for grade B BP monitor, the AAMI standards, and the IEEE standards for grade B BP monitor.
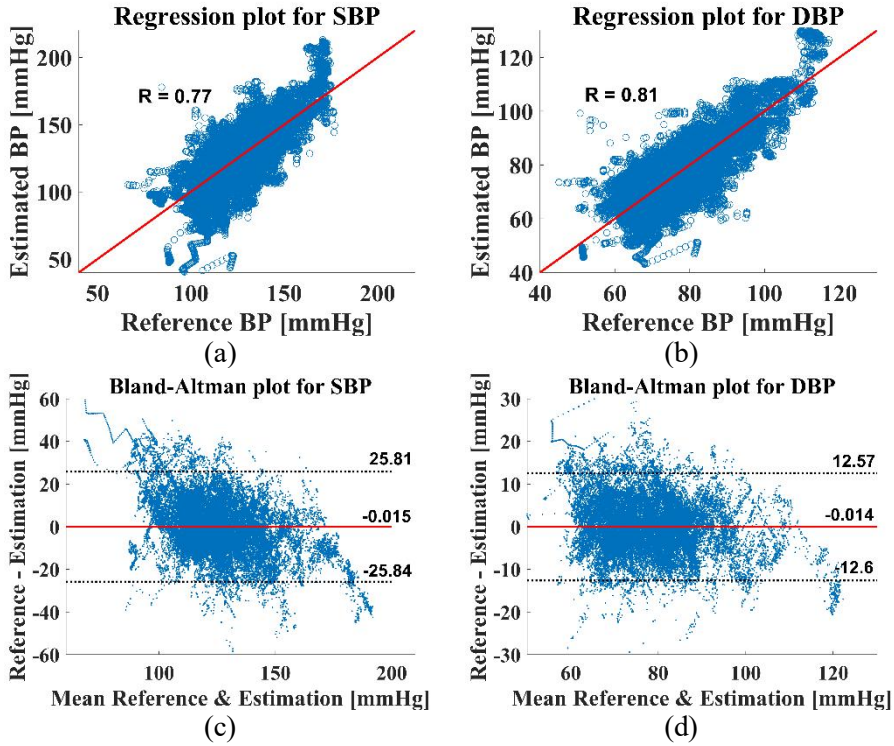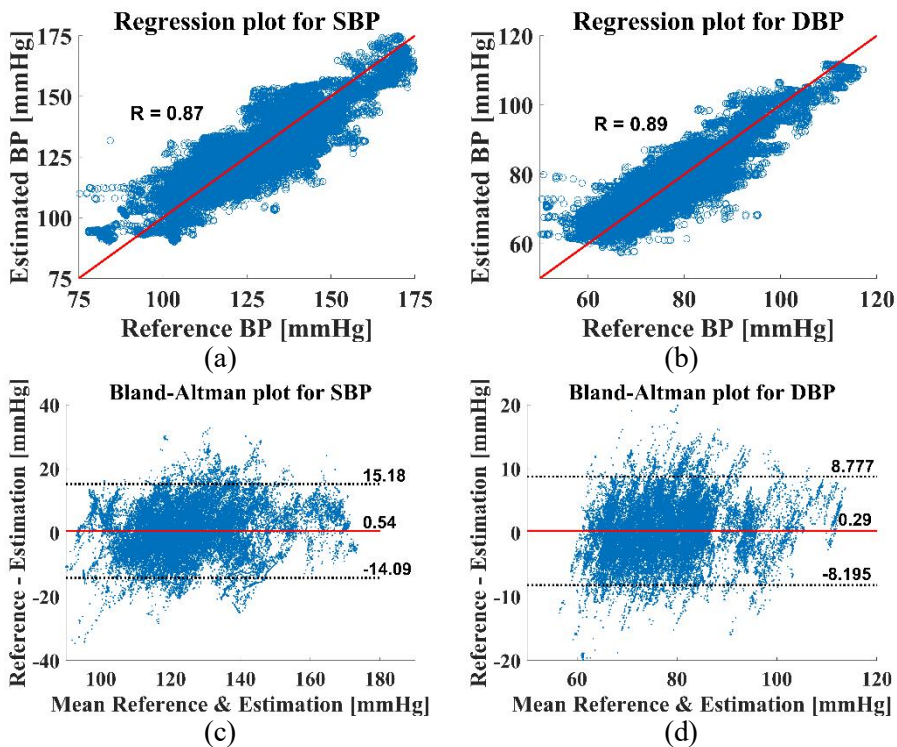

Figure 3.11 Performance of the BP estimation model across the single chest-worn device dataset with applying the transfer function. (a) Regression plot for

SBP estimation; (b) Regression plot for DBP estimation; (c) Bland-Altman plot for SBP estimation; (d) Bland-Altman plot for DBP estimation.

Table 3.3 Performance of the BP estimation model across the single chest-worn device dataset with applying the transfer function

Performance Measure	SBP estimation model		DBP estimation model	
	Value	Evaluation	Value	Evaluation
ME (mmHg)	0.54	**PASS[a]**	0.29	**PASS[a]**
SDE (mmHg)	7.47		4.33	
Cumulative Error < 5 mmHg (%)	52		77	
Cumulative Error < 10 mmHg (%)	82	**B[b]**	97	**A[b]**
Cumulative Error < 15 mmHg (%)	95		99	
MAD (mmHg)	5.86	**B[c]**	3.32	**A[c]**
Correlation to reference (mean $\pm$ STD)	0.49 $\pm$ 0.37		0.34 $\pm$ 0.45	

[a]Evaluation against the AAMI standards.
[b]Evaluation against the BHS BP monitor standards.
[c]Evaluation against the IEEE standards.

3.4.3 Comparison with the Previous Study using the Single Chest-worn Device

As described in 3.1, in our preliminary study for BP estimation using the developed single chest-worn device, a multivariate linear model using the SCG amplitude in conjunction with PTT trained in the dataset from 10 subjects was evaluated against 20 subjects [112]. Compared to the result of the previous study, BP estimation model developed in this study have several points of improvement in performance.

First, SCG signal was not used for BP estimation in this study. SCG, the local vibrations of the chest wall in response to the heartbeat, has gained wide

interest for providing rich information regarding cardiac motions [115]. Previous works have shown that a characteristic point of the SCG waveform coincides with the opening of the aortic valve [116], which can be used to detect the proximal timing for PTT calculation. In addition, the amplitude of the SCG waveform has been validated for estimating cardiac ejection [116, 117]. However, the SCG signal is very susceptible to motion artifacts and it is not clearly measured from some subjects with high body fat percentages due to low quality of the signals. Furthermore, the amplitude of the SCG waveform is highly variable depending on the measurement location or from subject to subject. Therefore, it is doubtful that any BP estimation method which use predictors extracted from the SCG signal could be accurate in a large sample.

Second, the BP estimation model in this study was constructed and validated in large open database to verify the model's applicability to large number of subjects and various subject phenotypes. The BP estimation model developed in the preliminary study was not extendable for general use since the small homogeneous subject pools are used to train and validate the model. However, the model in this study was trained and validated from more than 1000 subjects using the two surgical biosignal databases.

The comparisons of the estimation results of testing the models across the single chest-worn device dataset with the previous study are presented in Table 3.4. There are significant improvements in all of the performance measures using the model developed in this study.

Table 3.4 The comparison of the results of this work with the previous study

Performance Measure	Previous study		This work	
	Value	Evaluation	Value	Evaluation
SBP estimation model				
ME (mmHg)	3.31	**FAIL**[a]	0.54	**PASS**[a]
SDE (mmHg)	8.07		7.47	
Cumulative Error < 5 mmHg (%)	43		52	
Cumulative Error < 10 mmHg (%)	73	**C**[b]	82	**B**[b]
Cumulative Error < 15 mmHg (%)	91		95	
MAD (mmHg)	6.89	**C**[c]	5.86	**B**[c]
DBP estimation model				
ME (mmHg)	-0.18	**PASS**[a]	0.29	**PASS**[a]
SDE (mmHg)	5.08		4.33	
Cumulative Error < 5 mmHg (%)	75		77	
Cumulative Error < 10 mmHg (%)	94	**A**[b]	97	**A**[b]
Cumulative Error < 15 mmHg (%)	97		99	
MAD (mmHg)	3.66	**A**[b]	3.32	**A**[c]

[a]Evaluation against the AAMI standards.
[b]Evaluation against the BHS BP monitor standards.
[c]Evaluation against the IEEE standards.

3.4.4 Limitations

There are a few limitations to mention. First, although the BP estimation model used in this study was evaluated through large population in surgical biosignal databases, the number of subjects for testing the model as a form factor of single chest-worn device was small. Biosignal data using the wearable device was obtained from only 25 males in this study. Therefore, further study for evaluating the developed model from a much larger number of subjects including females should be needed in order to completely evaluate the applicability of the model to the single chest-worn device. In this case, the BP estimation model can be directly developed using ECG and chest PPG signal measured from the single chest-worn device from large heterogeneous subject

pools without applying the transfer function, which can further improve the estimation performance.

Another limitation is the small number of subjects used in transfer function model development. However, in this study, feature standardization was performed prior to inputting the PPG morphology features to the transfer function model for the purpose of minimizing intra-patient variability of the model. It can be deduced that generalizable transfer function is properly developed in this study since the estimation performance in test dataset is greatly improved by applying the transfer function derived from data independent to the test dataset.

Last limitation is the reference BP used in this study. As described in 3.2.3, Finometer continuous BP monitor, which was based on the volume clamp method, was used as a reference to obtain the device dataset in in-lab condition in this study. Although this method has been used in numerous previous studies for obtaining the reference BP since it can provide relatively accurate BP values continuously, these BP outputs are estimates, not representing accurate BP readings. According to the BHS, AAMI, and IEEE standards for BP monitors, the reference BP must be measured using intra-catheter BP or using auscultation with two separate observers who agree on the measured value. Therefore, further study is needed to validate the BP estimation model across the device dataset which includes the accurate reference BP measurements.

3.5 Conclusion

In conclusion, a single wireless chest-worn device with compact size, light weight, and low power consumption was developed to continuously measure ECG and PPG in order to realize continuous and long-term daily monitoring of BP. Furthermore, by developing the transfer function mapping the chest PPG morphology features to the corresponding finger PPG morphology features, the large population BP estimation model could be applied to the form factor of the single chest-worn device with satisfying the three relevant international standards for BP monitors.

Chapter 4

Thesis Summary and Future

Direction

4.1 Summary and Contributions

Currently, BP is measured through the insertion of a catheter into an artery, or measured by using cuff-based methods at the clinic. Although BP can be mostly accurately and continuously measured by using intra-arterial catheter method, this method is invasive, so it can be only employed in human under intensive care medicine, anesthesiology, or for research purposes. Cuff-based methods can provide non-invasive BP measurements with clinically acceptable accuracy. However, they can measure only a single discrete BP measurement, and they are not suitable for long-term daily BP monitoring due to their low user compliance. Therefore, the next generation of BP monitoring system should provide non-invasive continuous BP measurements both with clinically acceptable accuracy and with utmost convenience for long-term daily monitoring.

In the first study, we developed a clinically usable BP estimation model using large heterogeneous subject pools in surgical biosignal databases. Due to the limited number of subjects used in most previous studies for BP estimation, there has not been any research that definitively confirmed how BP related features such as PAT, PTT, and PPG morphology features actually relate to BP from a large diverse subject group. In this study, we used novel feature selection methods to validate the potential of these features as predictors of BP comprehensively from more than 1,000 surgical patients, and determined 28

features including several PPG morphology features and PAT as suitable BP predictors. Using the selected BP predictors, several modelling methods were tested in order to construct the clinically usable BP estimation model. In order to enhance estimation performance, frequency component separation method and non-linear regression methods based on ANN or RNN were performed. As a result, BP estimation models constructed by modelling low frequency component of BP using ANN and high frequency component using RNN with selected 28 predictors showed the best estimation performance, satisfying the three relevant international standards for BP monitors in validation and in external validation datasets.

In the second study, we developed an unobtrusive single wireless chest-worn device which facilitates long-term daily BP monitoring. Unlike most previous studies using two or more modules with bulky electrodes for signal acquisition, the developed device can measure ECG and PPG simultaneously from the torso to extract BP predictors with single compact size, light weight, and low power consumption for enhancing user compliance. Since the characteristics of PPG waveform from the chest were significantly different with those from the finger, the transfer function model which translates the chest PPG morphology features to the corresponding finger PPG morphology features were developed. By testing the clinically usable BP estimation model to the device dataset obtained from 25 subjects in three BP intervention

experiments, the model satisfied the three relevant international standards for BP monitors with applying the transfer function.

In conclusion, clinically usable and long-term daily monitoring non-invasive continuous arterial BP estimation system was developed and evaluated in multiple datasets in this study. This result can contribute to a more reliable assessment and management of the BP status for diagnosing and preventing hypertension in an early stage.

4.2 Future Work

In order to utilize the developed non-invasive continuous arterial BP monitoring system at the clinic, the system should output BP values in real-time. In this study, all of the processes to estimate BP including biosignal pre-processing, feature extraction, the transfer function model, and the BP estimation model based on ANN and RNN were performed in measured data retrospectively. Therefore, further software which performs all processes to estimate BP in pseudo real-time should be developed. It can be implemented in the single chest-worn device itself, or in a PC based program.

The developed single chest-worn BP monitoring device should be further enhanced for minimizing the user's discomfort. The current system requires a strap band wrapped around the torso to attach the device tightly to the chest, which leads to practical limit of the system. In order to solve it, the device should be developed in a self-adhesive form to freely attach and detach from the chest without strap band. For this, the device should be smaller and lighter. Although the device has compact size with 40 mm in length, 76 mm in width, and 18 mm in thickness, and has light weight with 27.5 g in current form, it can be more minimized with an advanced circuit and hard case design.

Finally, biosignal data using the developed device should be further obtained from large heterogeneous subject pool. As described in 3.4.4, the developed BP estimation model should be evaluated to the device dataset with

a much larger number of subjects including females in order to completely assess the applicability of the model to the form factor of single chest-worn device. Furthermore, for the purpose of utilizing the developed non-invasive continuous BP monitoring system in daily life or during surgery as alternative to intra-arterial catheter, the system needs to be evaluated from datasets containing various mechanisms of BP variation in less controlled environment with various postural changes.

Bibliography

[1]   W. H. Organization, "Cardiovascular Diseases," W. H. Organization, Ed., ed, 2015.

[2]   N. H. Flebach, P. R. Hebert, M. J. Stampfer, G. A. Colditz, W. C. Willett, B. Rosner, *et al.*, "A PROSPECTIVE STUDY OF HIGH BLOOD PRESSURE AND CARDIOVASCULAR DISEASE IN WOMEN," *American Journal of Epidemiology,* vol. 130, pp. 646-654, 1989.

[3]   S. MacMahon, R. Peto, R. Collins, J. Godwin, S. MacMahon, J. Cutler, *et al.*, "Blood pressure, stroke, and coronary heart disease: Part 1, prolonged differences in blood pressure: prospective observational studies corrected for the regression dilution bias," *The Lancet,* vol. 335, pp. 765-774, 1990/03/31/ 1990.

[4]   W. H. Organization, "A global brief on hypertension: silent killer, global public health crisis: World Health Day 2013," World Health Organization2013.

[5]   J. Stamler, R. Stamler, and J. D. Neaton, "Blood pressure, systolic and diastolic, and cardiovascular risks: Us population data," *Archives of Internal Medicine,* vol. 153, pp. 598-615, 1993.

[6]   P. K. Whelton, "Epidemiology of hypertension," *The Lancet,* vol. 344, pp. 101-106, 1994/07/09/ 1994.

[7]   P. K. Whelton, T. V. Perneger, F. L. Brancati, and M. J. Klag, "Epidemiology and prevention of blood pressure-related renal disease," *Journal of Hypertension,* vol. 10, p. S85, 1992.

[8]   P. K. Whelton, R. M. Carey, W. S. Aronow, D. E. Casey, K. J. Collins, C. D. Himmelfarb, *et al.*, "2017 ACC/AHA/AAPA/ABC/ACPM/AGS/APhA/ASH/ASPC/NMA/PCN A guideline for the prevention, detection, evaluation, and management of high blood pressure in adults: a report of the American College of Cardiology/American Heart Association Task

Force on Clinical Practice Guidelines," *Journal of the American College of Cardiology,* vol. 71, pp. e127-e248, 2018.

[9]   Y. Ostchega, C. D. Fryar, T. Nwankwo, and D. T. Nguyen, "Hypertension Prevalence Among Adults Aged 18 and Over: United States, 2017–2018," *NCHS Data Brief,* pp. 1-8, 2020.

[10]   V. L. Burt, P. Whelton, E. J. Roccella, C. Brown, J. A. Cutler, M. Higgins*, et al.*, "Prevalence of Hypertension in the US Adult Population," *Results From the Third National Health and Nutrition Examination Survey, 1988-1991,* vol. 25, pp. 305-313, 1995.

[11]   T. G. Pickering, J. E. Hall, L. J. Appel, B. E. Falkner, J. Graves, M. N. Hill*, et al.*, "Recommendations for blood pressure measurement in humans and experimental animals: part 1: blood pressure measurement in humans: a statement for professionals from the Subcommittee of Professional and Public Education of the American Heart Association Council on High Blood Pressure Research," *Hypertension,* vol. 45, pp. 142-161, 2005.

[12]   P. Armitage and G. A. Rose, "The variability of measurements of casual blood pressure. I. A laboratory study," *Clinical science,* vol. 30, pp. 325-335, 1966/04// 1966.

[13]   T. G. Pickering, G. A. Harshfield, R. B. Devereux, and J. H. Laragh, "What is the role of ambulatory blood pressure monitoring in the management of hypertensive patients?," *Hypertension,* vol. 7, pp. 171-177, 1985.

[14]   A. Frattola, G. Parati, C. Cuspidi, F. Albini, and G. Mancia, "Prognostic value of 24-hour blood pressure variability," *Journal of hypertension,* vol. 11, pp. 1133-1137, 1993.

[15]   P. Verdecchia, C. Porcellati, G. Schillaci, C. Borgioni, A. Ciucci, M. Battistelli*, et al.*, "Ambulatory blood pressure. An independent predictor of prognosis in essential hypertension," *Hypertension,* vol. 24, pp. 793-801, 1994.

[16]   M. Shinagawa, K. Otsuka, S. Murakami, Y. Kubo, G. Cornelissen, K. Matsubayashi*, et al.*, "Seven-day (24-h) ambulatory blood pressure

monitoring, self-reported depression and quality of life scores," *Blood pressure monitoring,* vol. 7, pp. 69-76, 2002.

[17]   S. P. Walker, M. J. Permezel, S. P. Brennecke, L. K. Tuttle, and J. R. Higgins, "Patient Satisfaction with the SpaceLabs 90207 Ambulatory Blood Pressure Monitor in Pregnancy," *Hypertension in Pregnancy,* vol. 23, pp. 295-301, 2004/01/01 2004.

[18]   V. Chandrasekaran, R. Dantu, S. Jonnada, S. Thiyagaraja, and K. P. Subbu, "Cuffless Differential Blood Pressure Estimation Using Smart Phones," *IEEE Transactions on Biomedical Engineering,* vol. 60, pp. 1080-1089, 2013.

[19]   W. Chen, T. Kobayashi, S. Ichikawa, Y. Takeuchi, and T. Togawa, "Continuous estimation of systolic blood pressure using the pulse arrival time and intermittent calibration," *Medical and Biological Engineering and Computing,* vol. 38, pp. 569-574, September 01 2000.

[20]   L. A. Geddes, M. H. Voelz, C. F. Babbs, J. D. Bourland, and W. A. Tacker, "Pulse Transit Time as an Indicator of Arterial Blood Pressure," *Psychophysiology,* vol. 18, pp. 71-74, 1981.

[21]   H. Gesche, D. Grosskurth, G. Küchler, and A. Patzak, "Continuous blood pressure measurement by using the pulse transit time: comparison to a cuff-based method," *European Journal of Applied Physiology,* vol. 112, pp. 309-315, January 01 2012.

[22]   S. Jae Hyuk, L. Kang Moo, and P. Kwang Suk, "Non-constrained monitoring of systolic blood pressure on a weighing scale," *Physiological Measurement,* vol. 30, p. 679, 2009.

[23]   F. Parry, G. Dumont, C. Ries, C. Mott, and M. Ansermino, "Continuous noninvasive blood pressure measurement by pulse transit time," in *The 26th Annual International Conference of the IEEE Engineering in Medicine and Biology Society*, 2004, pp. 738-741.

[24]   C. C. Y. Poon and Y. T. Zhang, "Cuff-less and Noninvasive Measurements of Arterial Blood Pressure by Pulse Transit Time," in *2005 IEEE Engineering in Medicine and Biology 27th Annual Conference*, 2005, pp. 5877-5880.

[25]   J. Solà, M. Proença, D. Ferrario, J. A. Porchet, A. Falhi, O. Grossenbacher*, et al.*, "Noninvasive and Nonocclusive Blood Pressure Estimation Via a Chest Sensor," *IEEE Transactions on Biomedical Engineering,* vol. 60, pp. 3505-3513, 2013.

[26]   E. S. Winokur, D. D. He, and C. G. Sodini, "A wearable vital signs monitor at the ear for continuous heart rate and Pulse Transit Time measurements," in *2012 Annual International Conference of the IEEE Engineering in Medicine and Biology Society*, 2012, pp. 2724-2727.

[27]   M. Y.-M. Wong, C. C.-Y. Poon, and Y.-T. Zhang, "An Evaluation of the Cuffless Blood Pressure Estimation Based on Pulse Transit Time Technique: a Half Year Study on Normotensive Subjects," *Cardiovascular Engineering,* vol. 9, pp. 32-38, March 01 2009.

[28]   J. C. Bramwell, "The velocity of pulse wave in man," *Proc. R. Soc. Lond. B,* vol. 93, pp. 298-306, 1922.

[29]   W. e. a. Nichols, *McDonald's Blood Flow In Arteries. Theoretical, Experimental and Clinical Principles*, 6 ed. London: Taylor & Francis, 2011.

[30]   A. I. Moens, *Die Pulscurve*: Brill, 1878.

[31]   A. I. Moens, *Over de voortplantingssnelheid van den pols*: SC Van Doesburgh, 1877.

[32]   D. Korteweg, "Ueber die Fortpflanzungsgeschwindigkeit des Schalles in elastischen Röhren," *Annalen der Physik,* vol. 241, pp. 525-542, 1878.

[33]   D. Hughes, C. F. Babbs, L. Geddes, and J. Bourland, "Measurements of Young's modulus of elasticity of the canine aorta with ultrasound," *Ultrasonic Imaging,* vol. 1, pp. 356-367, 1979.

[34]   F. S. Cattivelli and H. Garudadri, "Noninvasive cuffless estimation of blood pressure from pulse arrival time and heart rate with adaptive calibration," in *2009 Sixth international workshop on wearable and implantable body sensor networks*, 2009, pp. 114-119.

[35]   L. Geddes, M. Voelz, S. James, and D. Reiner, "Pulse arrival time as a method of obtaining systolic and diastolic blood pressure indirectly,"

Medical and Biological Engineering and Computing, vol. 19, pp. 671-672, 1981.

[36]   J. Muehlsteff, X. Aubert, and G. Morren, "Continuous cuff-less blood pressure monitoring based on the pulse arrival time approach: The impact of posture," in *2008 30th annual international conference of the IEEE Engineering in Medicine and Biology Society*, 2008, pp. 1691-1694.

[37]   Z. Tang, T. Tamura, M. Sekine, M. Huang, W. Chen, M. Yoshida*, et al.*, "A Chair-Based Unobtrusive Cuffless Blood Pressure Monitoring System Based on Pulse Arrival Time," *IEEE Journal of Biomedical and Health Informatics,* vol. 21, pp. 1194-1205, 2017.

[38]   X. Ding, B. P. Yan, Y.-T. Zhang, J. Liu, N. Zhao, and H. K. Tsang, "Pulse transit time based continuous cuffless blood pressure estimation: A new extension and a comprehensive evaluation," *Scientific reports,* vol. 7, p. 11554, 2017.

[39]   R. Mukkamala, J. O. Hahn, O. T. Inan, L. K. Mestha, C. S. Kim, H. Töreyin*, et al.*, "Toward Ubiquitous Blood Pressure Monitoring via Pulse Transit Time: Theory and Practice," *IEEE Transactions on Biomedical Engineering,* vol. 62, pp. 1879-1901, 2015.

[40]   S. Puke, T. Suzuki, K. Nakayama, H. Tanaka, and S. Minami, "Blood pressure estimation from pulse wave velocity measured on the chest," in *2013 35th Annual International Conference of the IEEE Engineering in Medicine and Biology Society (EMBC)*, 2013, pp. 6107-6110.

[41]   C.-S. Kim, S. L. Ober, M. S. McMurtry, B. A. Finegan, O. T. Inan, R. Mukkamala*, et al.*, "Ballistocardiogram: Mechanism and Potential for Unobtrusive Cardiovascular Health Monitoring," *Scientific Reports,* vol. 6, p. 31297, 08/09

05/09/received

07/15/accepted 2016.

[42]   C. Kim, A. M. Carek, O. T. Inan, R. Mukkamala, and J. Hahn, "Ballistocardiogram-Based Approach to Cuffless Blood Pressure Monitoring: Proof of Concept and Potential Challenges," *IEEE*

Transactions on Biomedical Engineering, vol. 65, pp. 2384-2391, 2018.

[43] J. Proença, J. Muehlsteff, X. Aubert, and P. Carvalho, "Is pulse transit time a good indicator of blood pressure changes during short physical exercise in a young population?," in *2010 Annual International Conference of the IEEE Engineering in Medicine and Biology*, 2010, pp. 598-601.

[44] L. Peter, N. Noury, and M. Cerny, "A review of methods for non-invasive and continuous blood pressure monitoring: Pulse transit time method is promising?," *IRBM,* vol. 35, pp. 271-282, 2014/10/01/ 2014.

[45] P. Su, X.-R. Ding, Y.-T. Zhang, J. Liu, F. Miao, and N. Zhao, "Long-term blood pressure prediction with deep recurrent neural networks," in *Biomedical & Health Informatics (BHI), 2018 IEEE EMBS International Conference on*, 2018, pp. 323-328.

[46] X. Teng and Y. Zhang, "Continuous and noninvasive estimation of arterial blood pressure using a photoplethysmographic approach," in *Engineering in Medicine and Biology Society, 2003. Proceedings of the 25th Annual International Conference of the IEEE*, 2003, pp. 3153-3156.

[47] W.-H. Lin, H. Wang, O. W. Samuel, G. Liu, Z. Huang, and G. Li, "New photoplethysmogram indicators for improving cuffless and continuous blood pressure estimation accuracy," *Physiological Measurement,* vol. 39, p. 025005, 2018/02/26 2018.

[48] F. Miao, N. Fu, Y. Zhang, X. Ding, X. Hong, Q. He*, et al.*, "A Novel Continuous Blood Pressure Estimation Approach Based on Data Mining Techniques," *IEEE Journal of Biomedical and Health Informatics,* vol. 21, pp. 1730-1740, 2017.

[49] X. Ding, Y. Zhang, J. Liu, W. Dai, and H. K. Tsang, "Continuous Cuffless Blood Pressure Estimation Using Pulse Transit Time and Photoplethysmogram Intensity Ratio," *IEEE Transactions on Biomedical Engineering,* vol. 63, pp. 964-972, 2016.

[50] S. G. Khalid, J. Zhang, F. Chen, and D. Zheng, "Blood Pressure Estimation Using Photoplethysmography Only: Comparison between Different Machine Learning Approaches," *Journal of Healthcare Engineering,* vol. 2018, p. 13, 2018.

[51] M. Radha, K. De Groot, N. Rajani, C. C. Wong, N. Kobold, V. Vos*, et al.*, "Estimating blood pressure trends and the nocturnal dip from photoplethysmography," *Physiological measurement,* vol. 40, p. 025006, 2019.

[52] Q. Liu, B. P. Yan, C.-M. Yu, Y.-T. Zhang, and C. C. Poon, "Attenuation of systolic blood pressure and pulse transit time hysteresis during exercise and recovery in cardiovascular patients," *IEEE Transactions on Biomedical Engineering,* vol. 61, pp. 346-352, 2013.

[53] X. Ding and Y. Zhang, "Photoplethysmogram intensity ratio: A potential indicator for improving the accuracy of PTT-based cuffless blood pressure estimation," in *2015 37th Annual International Conference of the IEEE Engineering in Medicine and Biology Society (EMBC)*, 2015, pp. 398-401.

[54] S. R. Alty, N. Angarita-Jaimes, S. C. Millasseau, and P. J. Chowienczyk, "Predicting arterial stiffness from the digital volume pulse waveform," *IEEE Transactions on Biomedical Engineering,* vol. 54, pp. 2268-2275, 2007.

[55] A. A. Awad, A. S. Haddadin, H. Tantawy, T. M. Badr, R. G. Stout, D. G. Silverman*, et al.*, "The relationship between the photoplethysmographic waveform and systemic vascular resistance," *Journal of Clinical Monitoring and Computing,* vol. 21, pp. 365-372, December 01 2007.

[56] L. Zhichang, Z. Song, Y. Wenming, and Y. Zibin, "A research on characteristic information of pulse wave," *Journal of Beijing Polytechnic University,* vol. 22, pp. 71-79, 1996.

[57] Y. S. Putyatina, "Measurement of arterial blood pressure by processing pulse wave data," in *Proceedings. 3rd Annual Siberian*

Russian Workshop on Electron Devices and Materials, 2002, pp. 77-78.

[58]   M. Elgendi, "On the analysis of fingertip photoplethysmogram signals," *Current cardiology reviews,* vol. 8, pp. 14-25, 2012.

[59]   M. Kachuee, M. M. Kiani, H. Mohammadzade, and M. Shabany, "Cuffless Blood Pressure Estimation Algorithms for Continuous Health-Care Monitoring," *IEEE Transactions on Biomedical Engineering,* vol. 64, pp. 859-869, 2017.

[60]   J. Feng, Z. Huang, C. Zhou, and X. Ye, "Study of continuous blood pressure estimation based on pulse transit time, heart rate and photoplethysmography-derived hemodynamic covariates," *Australasian physical & engineering sciences in medicine,* vol. 41, pp. 403-413, 2018.

[61]   J.-J. Huang, H.-Y. Syu, Z.-L. Cai, and A. R. See, "Development of a long term dynamic blood pressure monitoring system using cuff-less method and pulse transit time," *Measurement,* vol. 124, pp. 309-317, 2018.

[62]   T. H. Huynh, R. Jafari, and W.-Y. Chung, "Noninvasive cuffless blood pressure estimation using pulse transit time and impedance plethysmography," *IEEE Transactions on Biomedical Engineering,* vol. 66, pp. 967-976, 2018.

[63]   J. Lee, J. Sohn, J. Park, S. Yang, S. Lee, and H. C. Kim, "Novel blood pressure and pulse pressure estimation based on pulse transit time and stroke volume approximation," *Biomedical engineering online,* vol. 17, p. 81, 2018.

[64]   A. Rasool, M. Rafiq, A. Nasir, and F. M. Kashif, "Continuous and Noninvasive Blood Pressure Estimation by Two-Sensor Measurement of Pulse Transit Time," in *2018 14th International Conference on Emerging Technologies (ICET)*, 2018, pp. 1-5.

[65]   Y. Wang, Z. Liu, and S. Ma, "Cuff-less blood pressure measurement from dual-channel photoplethysmographic signals via peripheral pulse transit time with singular spectrum analysis," *Physiological measurement,* vol. 39, p. 025010, 2018.

[66]   E. Hietanen, "Cardiovascular responses to static exercise," *Scandinavian Journal of Work, Environment & Health,* vol. 10, pp. 397-402, 1984.

[67]   R. G. Haennel, G. D. Snydmiller, K. K. Teo, P. V. Greenwood, H. A. Quinney, and C. T. Kappagoda, "Changes in blood pressure and cardiac output during maximal isokinetic exercise," *Archives of physical medicine and rehabilitation,* vol. 73, pp. 150-155, 1992.

[68]   Y. Choi, Q. Zhang, and S. Ko, "Noninvasive cuffless blood pressure estimation using pulse transit time and Hilbert–Huang transform," *Computers & Electrical Engineering,* vol. 39, pp. 103-111, 2013.

[69]   J. C. Ruiz-Rodríguez, A. Ruiz-Sanmartín, V. Ribas, J. Caballero, A. García-Roche, J. Riera*, et al.*, "Innovative continuous non-invasive cuffless blood pressure monitoring based on photoplethysmography technology," *Intensive Care Medicine,* vol. 39, pp. 1618-1625, September 01 2013.

[70]   F. P.-W. Lo, C. X.-T. Li, J. Wang, J. Cheng, and M. Q.-H. Meng, "Continuous systolic and diastolic blood pressure estimation utilizing long short-term memory network," in *2017 39th Annual International Conference of the IEEE Engineering in Medicine and Biology Society (EMBC)*, 2017, pp. 1853-1856.

[71]   L. Wang, W. Zhou, Y. Xing, and X. Zhou, "A Novel Neural Network Model for Blood Pressure Estimation Using Photoplethesmography without Electrocardiogram," *Journal of healthcare engineering,* vol. 2018, 2018.

[72]   A. L. Goldberger, L. A. N. Amaral, L. Glass, J. M. Hausdorff, P. C. Ivanov, R. G. Mark*, et al.*, "PhysioBank, PhysioToolkit, and PhysioNet," *Components of a New Research Resource for Complex Physiologic Signals,* vol. 101, pp. e215-e220, 2000.

[73]   A. E. Johnson, T. J. Pollard, L. Shen, H. L. Li-wei, M. Feng, M. Ghassemi*, et al.*, "MIMIC-III, a freely accessible critical care database," *Scientific data,* vol. 3, p. 160035, 2016.

[74]   Y. Liang, D. Abbott, N. Howard, K. Lim, R. Ward, and M. Elgendi, "How effective is pulse arrival time for evaluating blood pressure?

Challenges and recommendations from a study using the MIMIC database," *Journal of clinical medicine,* vol. 8, p. 337, 2019.

[75]   R. A. Payne, C. N. Symeonides, D. J. Webb, and S. R. J. Maxwell, "Pulse transit time measured from the ECG: an unreliable marker of beat-to-beat blood pressure," *Journal of Applied Physiology,* vol. 100, pp. 136-141, 2006.

[76]   J. Muehlsteff, X. L. Aubert, and M. Schuett, "Cuffless Estimation of Systolic Blood Pressure for Short Effort Bicycle Tests: The Prominent Role of the Pre-Ejection Period," in *2006 International Conference of the IEEE Engineering in Medicine and Biology Society*, 2006, pp. 5088-5092.

[77]   M. Y. M. Wong, E. Pickwell-MacPherson, Y. T. Zhang, and J. C. Cheng, "The effects of pre-ejection period on post-exercise systolic blood pressure estimation using the pulse arrival time technique," *European journal of applied physiology,* vol. 111, pp. 135-144, 2011.

[78]   H.-C. Lee and C.-W. Jung, "Vital Recorder-a free research tool for automatic recording of high-resolution time-synchronised physiological data from multiple anaesthesia devices," *Scientific reports,* vol. 8, pp. 1527-1527, 2018.

[79]   J. M. Łęski and N. Henzel, "ECG baseline wander and powerline interference reduction using nonlinear filter bank," *Signal processing,* vol. 85, pp. 781-793, 2005.

[80]   J. Pan and W. J. Tompkins, "A Real-Time QRS Detection Algorithm," *IEEE Transactions on Biomedical Engineering,* vol. BME-32, pp. 230-236, 1985.

[81]   N. Gaddum, J. Alastruey, P. Beerbaum, P. Chowienczyk, and T. Schaeffter, "A technical assessment of pulse wave velocity algorithms applied to non-invasive arterial waveforms," *Annals of biomedical engineering,* vol. 41, pp. 2617-2629, 2013.

[82]   X. Ding and Y.-T. Zhang, "Pulse transit time technique for cuffless unobtrusive blood pressure measurement: from theory to algorithm," *Biomedical Engineering Letters,* vol. 9, pp. 37-52, February 01 2019.

[83]   Y. Kurylyak, F. Lamonaca, and D. Grimaldi, "A Neural Network-based method for continuous blood pressure estimation from a PPG signal," in *2013 IEEE International Instrumentation and Measurement Technology Conference (I2MTC)*, 2013, pp. 280-283.

[84]   K. Takazawa, N. Tanaka, M. Fujita, O. Matsuoka, T. Saiki, M. Aikawa*, et al.*, "Assessment of Vasoactive Agents and Vascular Aging by the Second Derivative of Photoplethysmogram Waveform," *Hypertension,* vol. 32, pp. 365-370, 1998.

[85]   A. John, "Photoplethysmography and its application in clinical physiological measurement," *Physiological Measurement,* vol. 28, p. R1, 2007.

[86]   M. Sherebrin and R. Sherebrin, "Frequency analysis of the peripheral pulse wave detected in the finger with a photoplethysmograph," *IEEE Transactions on biomedical engineering,* vol. 37, pp. 313-317, 1990.

[87]   S. Millasseau, R. Kelly, J. Ritter, and P. Chowienczyk, "Determination of age-related increases in large artery stiffness by digital pulse contour analysis," *Clinical science,* vol. 103, pp. 371-377, 2002.

[88]   I. Guyon and A. Elisseeff, "An introduction to variable and feature selection," *Journal of machine learning research,* vol. 3, pp. 1157-1182, 2003.

[89]   N. Meinshausen and P. Bühlmann, "Stability selection," *Journal of the Royal Statistical Society: Series B (Statistical Methodology),* vol. 72, pp. 417-473, 2010.

[90]   D. W. Marquardt and R. D. Snee, "Ridge regression in practice," *The American Statistician,* vol. 29, pp. 3-20, 1975.

[91]   U. M. Khaire and R. Dhanalakshmi, "Stability of feature selection algorithm: A review," *Journal of King Saud University - Computer and Information Sciences,* 2019/06/25/ 2019.

[92]   B. C. Ross, "Mutual information between discrete and continuous data sets," *PloS one,* vol. 9, 2014.

[93]   I. Guyon, J. Weston, S. Barnhill, and V. Vapnik, "Gene selection for cancer classification using support vector machines," *Machine learning,* vol. 46, pp. 389-422, 2002.

[94] T. K. Ho, "Random decision forests," in *Proceedings of 3rd international conference on document analysis and recognition*, 1995, pp. 278-282.

[95] H. Peng, F. Long, and C. Ding, "Feature selection based on mutual information criteria of max-dependency, max-relevance, and min-redundancy," *IEEE Transactions on pattern analysis and machine intelligence,* vol. 27, pp. 1226-1238, 2005.

[96] P. Geurts, D. Ernst, and L. Wehenkel, "Extremely Randomized Trees," *Machine Learning,* vol. 63, pp. 3-42, 04/01 2006.

[97] R. J. Williams and D. Zipser, "A learning algorithm for continually running fully recurrent neural networks," *Neural computation,* vol. 1, pp. 270-280, 1989.

[98] S. Hochreiter and J. Schmidhuber, "Long short-term memory," *Neural computation,* vol. 9, pp. 1735-1780, 1997.

[99] M. Schuster and K. K. Paliwal, "Bidirectional recurrent neural networks," *IEEE Transactions on Signal Processing,* vol. 45, pp. 2673-2681, 1997.

[100] A. f. t. A. o. M. Instrumentation, "American national standard. Electronic or automated sphygmomanometers," *ANSI/AAMI SP10-1992/A1,* 1996.

[101] E. O'Brien, J. Petrie, W. Littler, M. de Swiet, P. L. Padfield, D. Altman*, et al.*, "The British Hypertension Society protocol for the evaluation of blood pressure measuring devices," *J hypertens,* vol. 11, pp. S43-S62, 1993.

[102] I. S. Association, "IEEE standard for wearable cuffless blood pressure measuring devices," *IEEE Std,* pp. 1708-2014, 2014.

[103] G. Zhang, M. Gao, D. Xu, N. B. Olivier, and R. Mukkamala, "Pulse arrival time is not an adequate surrogate for pulse transit time as a marker of blood pressure," *Journal of Applied Physiology,* vol. 111, pp. 1681-1686, 2011.

[104] J. Lee, S. Yang, S. Lee, and H. C. Kim, "Analysis of Pulse Arrival Time as an Indicator of Blood Pressure in a Large Surgical Biosignal Database: Recommendations for Developing Ubiquitous Blood

Pressure Monitoring Methods," *Journal of clinical medicine,* vol. 8, p. 1773, 2019.

[105] S. Li, W. Li, C. Cook, C. Zhu, and Y. Gao, "Independently recurrent neural network (indrnn): Building a longer and deeper rnn," in *Proceedings of the IEEE conference on computer vision and pattern recognition*, 2018, pp. 5457-5466.

[106] R. M. Carey and P. K. Whelton, "Prevention, detection, evaluation, and management of high blood pressure in adults: synopsis of the 2017 American College of Cardiology/American Heart Association Hypertension Guideline," *Annals of internal medicine,* vol. 168, pp. 351-358, 2018.

[107] A. E. W. Johnson, T. J. Pollard, L. Shen, L.-w. H. Lehman, M. Feng, M. Ghassemi*, et al.*, "MIMIC-III, a freely accessible critical care database," *Scientific Data,* vol. 3, p. 160035, 05/24/online 2016.

[108] S. P. Linder, S. M. Wendelken, E. Wei, and S. P. McGrath, "Using the morphology of photoplethysmogram peaks to detect changes in posture," *Journal of clinical monitoring and computing,* vol. 20, pp. 151-158, 2006.

[109] S. Yang, J. Sohn, S. Lee, J. Lee, and H. C. Kim, "Estimation and Validation of Arterial Blood Pressure using Photoplethysmogram Morphology Features in conjunction with Pulse Arrival Time in Large Open Databases," *IEEE Journal of Biomedical and Health Informatics,* 2020.

[110] C. Douniama, C. Sauter, and R. Couronne, "Blood pressure tracking capabilities of pulse transit times in different arterial segments: a clinical evaluation," in *2009 36th Annual Computers in Cardiology Conference (CinC)*, 2009, pp. 201-204.

[111] J. Y. A. Foo and C. S. Lim, "Dual-channel photoplethysmography to monitor local changes in vascular stiffness," *Journal of clinical monitoring and computing,* vol. 20, pp. 221-227, 2006.

[112] J. Park, S. Yang, J. Sohn, J. Lee, S. Lee, Y. Ku*, et al.*, "Cuffless and Continuous Blood Pressure Monitoring Using a Single Chest-Worn Device," *IEEE Access,* vol. 7, pp. 135231-135246, 2019.

[113] M. Al'Absi, S. Bongard, T. Buchanan, G. A. Pincomb, J. Licinio, and W. R. Lovallo, "Cardiovascular and neuroendocrine adjustment to public speaking and mental arithmetic stressors," *Psychophysiology,* vol. 34, pp. 266-275, 1997.

[114] L. Mourot, M. Bouhaddi, and J. Regnard, "Effects of the cold pressor test on cardiac autonomic control in normal subjects," *Physiological research,* vol. 58, 2009.

[115] O. T. Inan, P. F. Migeotte, K. S. Park, M. Etemadi, K. Tavakolian, R. Casanella*, et al.*, "Ballistocardiography and Seismocardiography: A Review of Recent Advances," *IEEE Journal of Biomedical and Health Informatics,* vol. 19, pp. 1414-1427, 2015.

[116] K. Tavakolian, "Characterization and analysis of seismocardiogram for estimation of hemodynamic parameters," Applied Science: School of Engineering Science, 2010.

[117] K. Tavakolian, A. P. Blaber, B. Ngai, and B. Kaminska, "Estimation of hemodynamic parameters from seismocardiogram," in *2010 Computing in Cardiology*, 2010, pp. 1055-1058.

Abstract in Korean

국문 초록

최근 수십 년 동안 비침습적 연속 혈압 모니터링에 대한 필요성이 점차 대두되면서 맥파 전달 시간, 맥파 도달 시간, 또는 광용적맥파의 파형으로부터 추출된 다양한 특징들을 이용한 혈압 추정 연구들이 전세계적으로 활발하게 진행되었다. 하지만 대부분의 연구들은 국제 혈압 표준을 만족시키지 못하는 매우 적은 수의 피험자들 만을 대상으로 주로 혈압 추정 모델을 개발 및 검증하였기 때문에 성능의 정확도가 적절하게 검증되지 못했다는 한계점이 있었고, 또한 혈압 추정 파라미터 추출을 위한 생체 신호들을 측정하기 위해 대부분 두 개 이상의 모듈을 필요로 하면서 실용성 측면에서 한계점이 있었다.

첫 번째 연구는 대규모 생체신호 데이터베이스들을 분석함으로써 임상적으로 허용 가능한 수준의 정확도가 적절히 검증된 혈압 추정 모델을 개발하는 것을 목적으로 진행되었다. 본 연구에서는 1376 명의 수술 중 환자들의 약 250 만 심박 주기에 대해 측정된 두 가지 비침습적 생체신호인 심전도와 광용적맥파를 활용한 혈압 추정 방식들을 분석하였다. 맥파 도달 시간, 심박수, 그리고 다양한 광용적맥파 파형 피처들을 포함하는 총 42 종류의 파라미터들을 대상으로 피처 선택 기법들을 적용한 결과, 28 개의 피처들이 혈압 추정 파라미터로 결정되었고, 특히 두 가지

광용적맥파 피처들이 기존에 혈압 추정 파라미터로 가장 주요하게 활용되었던 맥파 도달 시간보다 우월한 파라미터들로 분석되었다. 선정된 파라미터들을 활용하여 혈압의 낮은 주파수 성분을 인공신경망으로 모델링하고, 높은 주파수 성분을 순환신경망으로 모델링 한 결과, 수축기 혈압 에러율 0.05 ± 6.92 mmHg 와 이완기 혈압 에러율 -0.05 ± 3.99 mmHg 정도의 높은 정확도를 달성하였다. 또 다른 생체신호 데이터베이스에서 추출한 334 명의 중환자들을 대상으로 모델을 외부 검증했을 때 유사한 결과를 획득하면서 세 가지 대표적 혈압 측정 장비 기준들을 모두 만족시켰다. 해당 결과를 통해 제안된 혈압 추정 모델이 1000 명 이상의 다양한 피험자들을 대상으로 적용 가능함을 확인하였다.

두 번째 연구는 일상 생활 중 장기간 모니터링이 가능한 단일 착용형 혈압 모니터링 시스템을 개발하는 것을 목적으로 진행되었다. 대부분의 기존 혈압 추정 연구들은 혈압 추정 파라미터 추출을 위해 필요한 생체신호들을 측정하기 위해 두 군데 이상의 신체 지점에 두 개 이상의 모듈을 부착하는 등 실용성 측면에서 한계를 나타냈다. 이를 해결하기 위해 본 연구에서는 심전도와 광용적맥파를 동시에 연속적으로 측정하는 단일 가슴 착용형 디바이스를 개발하였고, 개발된 디바이스를 대상으로 총 25 명의 건강한 피험자들로부터 데이터를 획득하였다. 손가락에서 측정된 광용적맥파와 가슴에서 측정된 광용적맥파 간 파형의 특성에 유의미한 차이가 있기 때문에 가슴에서 측정된 광용적맥파에서

추출된 피처들을 대응되는 손가락에서 측정된 광용적맥파 피처들로 특성을 변환하는 전달 함수 모델을 개발하였다. 25 명으로부터 획득한 데이터에 전달 함수 모델을 적용시킨 후 혈압 추정 모델을 검증한 결과, 수축기 혈압 에러율 0.54 ± 7.47 mmHg 와 이완기 혈압 에러율 0.29 ± 4.33 mmHg 로 나타나면서 세 가지 혈압 측정 장비 기준들을 모두 만족시켰다.

결론적으로 본 연구에서는 임상적으로 허용 가능한 수준의 정확도로 장기간 일상 생활이 가능한 비침습적 연속 동맥 혈압 모니터링 시스템을 개발하고 다수의 데이터셋을 대상으로 검증함으로써 고혈압 조기 진단 및 예방을 위한 모바일 헬스케어 서비스의 가능성을 확인하였다.

주요어: 혈압, 연속 혈압 모니터링, 생체신호 데이터베이스, 광용적맥파, 맥파 전달 시간, 웨어러블 디바이스, 모바일 헬스케어

학 번: 2016-21173

Acknowledgement

MELAB 연구실에서 함께 지냈던 선배, 후배, 동료 연구원 분들께도 감사 드립니다. 부족한 저를 챙겨주시고 이끌어주신 선배님들이신 윤서 형, 지흠 누나, 병욱이 형, 진우 형, 중우 형, 준녕이 형, 종현이 형, 지수 누나, 도윤이 형, 동헌이 형께 감사 드리고, 함께 오랜 시간 연구실 생활을 같이 하면서 지낸 희진이 형, 치헌이 형, 석규, 희안 누나, 장재 형, 순빈, 지은이에게 고맙습니다. 특히 혈압 연구를 비롯하여 함께 다양한 연구들을 수행하면서 많은 도움을 주신 준녕이 형과 종현이 형에게 다시 한번 감사의 말씀을 전하고, 연구실 생활하면서 가장 많이 교류하고 정신적인 지지를 보내준 동기인 장재 형에게 특별히 고마움을 전하고 싶습니다.

마지막으로 제가 무사히 박사 학위 과정을 마칠 수 있도록 묵묵히 뒤에서 지켜봐 주시고 기도해주신 저의 가족들에게 진심으로 감사의 말씀을 전합니다. 저의 행복을 위해 매일 기도해주시고 보살펴주시는 어머니, 아버지께 감사 드리고, 그 동안 학생이라는 핑계로 제대로 효도해 드리지 못해 죄송합니다. 저를 믿고 지지해주신 만큼 앞으로 더욱 자랑스러운 아들이 되어 효도하겠습니다. 저를 위해 기도해준 큰누나, 작은누나, 매형들께도 감사의 말씀을 전합니다.

2021 년 2 월 양승만 올림